Feyerabend, F.; Druecker, H.; Laipple, D.; Vogt, C.; Stekker, M.; Hort, N.; Willumeit, R.:

Ion release from magnesium materials in physiological solutions under different oxygen tensions

In: Journal of Materials Science: Materials in Medicine (2011) Springer

DOI: 10.1007/s10856-011-4490-5

Ion release from magnesium materials in physiological solutions under different oxygen tensions

Frank Feyerabend [a*], Heiko Drücker [b*], Daniel Laipple [a], Carla Vogt [b], Michael Stekker [c], Norbert Hort [a], Regine Willumeit [a]

[a] Helmholtz-Zentrum Geesthacht, Institute of Materials Research, Max-Planck-Str. 1, D - 21502 Geesthacht, Germany

[b] Institute for Inorganic Chemistry, Leibniz University of Hannover, Callinstr. 9, 30167 Hannover, Germany

c MeKo, Im Kirchenfelde 12-14, 31157 Sarstedt / Hannover, Germany

* Both authors have contributed equivalently.

Correspondence:

Dr. Frank Feyerabend, Helmholtz-Zentrum Geesthacht, Institute for Material Research, Department of Macromolecular Structure Research, Max-Planck-Str. 1, 21502 Geesthacht, Germany.

Phone: 0049 4152 87 1259, Fax: 0049 4152 87 2595

email: frank.feyerabend@hzg.de

Keywords

Magnesium, corrosion, proteins, oxygen, ion release

Abstract

Although magnesium as degradable biomaterial already showed clinical proof of concepts, the design of new alloys requires predictive *in vitro* methods, which are still lacking. Incubation under cell culture conditions to obtain “physiological” corrosion may be a solution. The aim of this study was to analyse the influence of different solutions, addition of proteins and of oxygen availability on the corrosion of different magnesium materials (pure Mg, WE43 and E11) with different surface finishing. Oxygen content in solution, pH, osmolality and ion relase were determined. Corrosion led to a reduction of oxygen in solution. The influence of oxygen on pH was enhanced by proteins, while osmolality was not influenced. Magnesium ion release was solution-dependent and enhanced in the initial phase by proteins with delayed release of alloying elements. The main corrosion product formed was magnesium carbonate. Therefore, cell culture conditions are proposed as first step toward physiological corrosion.

Introduction

Magnesium in biomedical applications has a long standing history and already showed different proof of concepts for medical applications [1]. However, besides of stent applications [2-5] there is no further clinical application yet. Although orthopaedic or paediatric applications would be of high interest, the approaches are hampered by the lack of suitable and predictive *in vitro* systems [6]. The comparison of *in vitro* and *in vivo* results usually differs by orders of magnitude [7], and the used setups are manifold and even not comparable *in vitro* [8]. Towards a reliable setup many factors have to be taken into account – tissue specific environment, the contact with blood and last but not least the contact with different, tissue-specific cell types. A first step for defining a relevant degradation model using cell culture conditions were performed recently [9, 10]. Here it was shown that the introduction of CO_2 led to a change in the formed corrosion products. Next to $Mg(OH)_2$, which

is the undisputed corrosion product in technical setups, under cell culture conditions mainly $MgCO_3$ is formed, which was also confirmed by other authors [11].

To shed a light on further aspects of the corrosion environment this study was performed regarding the availability of oxygen and proteins. Proteins are ubiquitous in the human body, whereas the amount of oxygen varies tissue-specifically between low oxygen conditions (<1%) in e.g. cartilage [12, 13] and normoxic (21%) conditions in arterial blood. The amount of available oxygen is important for cellular differentiation [14]. In this study the effect of the addition of proteins and the variation of available oxygen was analysed.

Moreover, it is known that the type of alloy and the preparation of the samples have an influence on the corrosion properties of the material, therefore three different alloys and three surface conditions were analyzed. The last aim of the study was to determine an optimal corrosion solution for the used setup; therefore a slightly buffered salt solution was compared to cell culture solution, which has even higher buffering capacity than whole blood.

Materials and Methods

Permanent mould casting of pure Magnesium and magnesium alloys WE43 and E11

Magnesium castings were prepared by pure Mg (99,95 wt.%) and pure alloying elements in a mild steel crucible under a cover gas mixture of Ar_2 and 0.3 % SF_6. After mixing at 730°C for 1.5 h, the alloy was cast to the mould preheated at 500 °C. The filled mould was held at 670 °C for 1 h under protective gas (Ar + 0.3 % SF_6. Then, the whole steel crucible with the melt was immersed into the continuous cooling water at 10 mm/s. When the bottom of steel crucible touched the water, it stopped for 1 second. As soon as the liquid level of inside melt was in alignment with the height of outside water, the solidification process was finished. The size of the ingot was 6 cm × 12 cm × 20 cm.

Based on earlier analyses of a commercially available WE43 alloy [15] the main components were used to have a more defined alloy composition. Therefore the cast alloy had the composition Mg -4 wt% Yttrium -0.5 wt% Gadolinium – 2 wt% Neodymium - 0.5 wt% Dysprosium (Mg4Y0.5Gd2Nd0.5Dy). The E11 alloy had the composition Mg10Gd1Nd.

Sample preparation and surface finishing

The ingots were cut by electrical discharge machining into plates (20 cm x 12 cm x 2 cm) and cylindrical samples (5 mm diameter) were prepared by laser cutting. Surface finishing was done by three different methods: 1. as cut (eroded surface); 2. electro polished and 3. etched.

Specimen sterilization

The samples were sonificated for 20 min in dry isopropanol, dried and gamma-sterilized at the In Core Irradiation (ICI) facility of the Geesthacht neutron facility with a total dosage of 29 kGy.

Composition of corrosion media

Two different solutions were used for the corrosion tests: I. Hanks balanced salt solution without calcium and magnesium (HBSS, Invitrogen Corporation, Karlsruhe, Germany) and II. Dulbecco's modified eagle medium Glutamax-I (DMEM, Invitrogen Corporation, Karlsruhe, Germany). The composition of the different corrosion media is depicted in Table 1. As additional experiment to determine the influence of proteins all solutions were supplemented with standardized 10 % foetal bovine serum (FBS, PAA Laboratories, Linz, Austria).

Corrosion environment

All corrosion experiments were carried out at 37°C, 5% CO_2 and 95% humidity in an incubator (Heraeus BBD 6620, Thermo Fisher Scientific, Schwerte, Germany), oxygen content was either set to 20 % or 5 %.The exposition time of the samples was at least 72 hours.

Online pH and oxygen measurement

The dynamic pH / oxygen measurement was performed with the SDR SensorDish Reader system (PreSens GmbH, Regensburg, Germany) on special 24-well-plates with an integrated pH sensor (multidish "HydroDish" or "OxyDish", PreSens GmbH, Regensburg, Germany). The measurement is based on non-invasive luminescence detection. The measurement range for pH determination of the system is limited from 4 to 9. Experiments were performed by incubating 5 mm magnesium samples in 1.5 mL of the respective corrosion media for 3

days with a medium change every 24 hours. Prior to discarding the medium was analysed further for pH after shaking (pH-meter Titan X, Fisher Scientific GmbH, Schwerte, Germany) as comparison to the online measurement, osmolality and ion release from the magnesium samples (see below). Oxygen measurements were performed in 4 replicates

Osmolality measurement

The corrosion solutions were replaced every 24 hours and analyzed for osmolality. Solutions kept under the same conditions but without magnesium sample served as reference. The osmolality was measured using an osmometer (Osmomat 030, Gonotec, Berlin, Germany). All corrosion media supplemented with 5 to 50 mM $MgCl_2$ (in steps of 5 mM) were measured as calibration to calculate the final molarity of the solutions out of the osmolality data.

Quantitative magnesium ion release measured by ICP-OES

To quantitatively determine the release of magnesium ions in the different corrosion media the resulting solutions hours were completely transferred to 15 mL Falcon tubes (Greiner Bio-One, Frickenhausen, Germany) after 24, 48 and 72 hours. The samples were diluted with ultrapure water and nitric acid (subboiled, 65 %) to a mass of about 11 g containing 2 weight-% acid and measured by ICP-OES (Arcos, Spectro Analytical Instruments, Kleve, Germany). In case of the addition of FBS, a formation of a precipitate was observed after addition of water and acid. This precipitate was dissolved by incubation for 3 weeks in an oven at 60 °C. The magnesium concentration in the media (DMEM and FBS) was determined and substracted, so all presented magnesium contents result from the corrosion process. All determinations were performed by analysis of two interference-free wavelengths including a drift correction.

Microscopy

Samples were rinsed after immersion for one minute in distilled water and dried in a vacuum oven for 24 hours. The corrosion layers were vizualized by scanning electron microscope (SEM; Auriga, Zeiss, Oberkochen, Germany). Images were taken at an accelerating voltage

of 5 keV with the secondary electron detector (SE2). Element analysis on the sample surface was performed by electron-dispersive x-ray spectroscopy (EDS; Apollo XP, EDAX, Ametek GmbH, Wiesbaden, Germany). The measurements were done standardless.

Cross-section specimens were cut using a diamond wire, embedded in a resin and polished with alumina. The final polishing was undertaken with a 0.1 lm colloidal silica suspension. Tthe not conductive epoxide resin samples had to be coated with a Gold-Palladium alloy to allow SEM investigations (SCD 030, Balzers Union, Balzer, Liechtenstein). To equal the deposit thickness of the sputtered coating, each pair was exposed to 30mA for a time of 60s. SEM-images were taken at 20kV accelerating voltage with the Back-Scattered-Electrons (BSE) - detector in order to gain material contrast. Due to obtain a high counting rate by EDS the SEM aperture of 120µm diameter had been used in High Current mode. EDS - mapping was realized on any sample with ever 9 regions of interest in the respective EDS spectrum; i.e. Mg, N, Na, C, Ca, Cl, K, O and P; to identify the element distribution of the corrosion layer. For every image at least 32 frames were mapped, each with a resolution of 512 x 400 points with a dwell time of 500µs per point. During EDS - mapping drift correction was applied to increase quality.

Statistical analysis

Statistics were performed using the SigmaStat package (Systat software GmbH, Erkrath, Germany). Standard analysis comparing more than two treatments was done by using the one-way ANOVA. Depending on the data distribution either a one-way ANOVA or an ANOVA on ranks was performed. Post-hoc tests were Holm-Sidak or Dunn’s multiple comparison, respectively. Statistical values are indicated at the relevant experiments.

Results

Effect of magnesium corrosion on oxygen tension

In contrast to technical corrosion setups where oxygen does not play a major role, the influence of oxygen on magnesium corrosion in physiological environments was not yet analysed. Due to the different availability of oxygen in tissues it may also be a relevant factor. Therefore we analysed the influence of oxygen tension on magnesium corrosion. The

average values (Table 2) showed a lower decrease at 5% that at 21% oxygen. However, the time-resolved oxygen measurements revealed different patterns of influence on the oxygen tension of the corroding magnesium. During incubation in 21 % oxygen and HBSS magnesium corrosion induced an initial drop of oxygen tension of about 9 %. A further decrease was observable starting at about 30 hours. After 66 hours the difference to control medium was only 1 %. The addition of proteins increased this difference slightly (mean reduction HBSS: 67.6 %; HBSS + FBS: 66 %). The incubation in 5 % O_2 led to lower decrease of 2.3 %, the minimum was reached at 12 hours, and thereafter the oxygen tension was slowly but constantly increasing. The addition of proteins accelerated this process (Figure 1a). To obtain a better overview the differences were depicted as percent reduction (Figure 1b). The curves showed no big differences, except for 5 % oxygen + FBS, were after about 30 hours the reduction decreased sharply. In contrast, the incubation with DMEM at 21 % O_2 showed an enduring decrease of oxygen in the range of 9 - 10 % and proteins enhanced the decrease up to 40 hours. This was also observable for the incubation at 5 % O_2, where the decrease was nearly stable up to 60 hours, thereafter the oxygen reduction became lower. Proteins induced a lower reduction of oxygen (Figure 1c and d).

Figure 1

Effect of magnesium corrosion and oxygen content on pH

The measurement of pH in the vicinity of the samples is a measure for the corrosion speed. While high pH indicates a fast corrosion (often due to pitting corrosion), lower pH indicates that either corrosion is more uniform or reduced. Therefore we measured pH online in the vicinity of the samples to have an indication about the course of corrosion.

The measurement of pH in the vicinity of the corroding samples showed some general trends as depicted in Figure 2. To determine the influence of proteins the ratio of average pH with and without the addition of FBS was calculated. It could be shown that the addition of proteins led to decrease in average pH in most of the cases (6 of 9 cases for each environment), except for the treatment with DMEM at 5 % O_2, where in only 2 out of 9 cases the addition of proteins reduced the average pH (Figure 2a). A clearer trend could be

observed when comparing the incubation in 5 and 21% oxygen. The reduction of oxygen in the gaseous phase to 5% led to a significant decrease of pH in DMEM (all surface conditions), with the addition of proteins in most cases (5 out of 9; Figure 2b).

Figure 2

Increase in osmolality

As a further measure of corrosion speed the osmolality was determined. In this case only the corrosion solutions containing 10 % FBS were analysed. Generally, the pure solutions had an initial osmolality of 0.257 Osm/Kg (HBSS) and 0.308 Osm/Kg (DMEM). To directly compare the different solutions the increase in osmolality with increasing immersion time was calculated (see Figure 3). Generally, the amount of oxygen was not influencing the osmolality of the solutions. Immersion in HBSS always led to a faster increase of osmolality compared to DMEM and the values were building a “plateau” after some time. In contrast, immersion in DMEM showed a lag phase with slow increase of osmolality up to 48 hours, but thereafter an increase to the level reached by the immersion in HBSS. The comparison of the different materials showed that pure magnesium induced the lowest increase, followed by WE43 and E11.

Figure 3

Ion release from the different materials

Ion release from the different materials was determined by ICP-OES. Some general trends were observable: (1) immersion in DMEM always led to lower ion release compared to HBSS; (2) The addition of FBS increased the amount of released magnesium in most cases and (3) alloying elements show a different release kinetic than magnesium (Figure 4). Moreover, it could be observed for most of the cases that a reduction in oxygen at least for the DMEM-solution reduced the ion release of magnesium ions.

Figure 4

Ion release due to surface conditions

The cumulative ion release from the different alloys and the different surface conditions is depicted in table 3. It could be observed, that the polished condition led to the slowest corrosion rates (determined by the ion release) in the pure magnesium samples. The alloy WE43 showed generally the highest corrosion rates and very inhomogeneous results. Moreover, some of the WE43 samples disintegrated already during the 3 days immersion experiments. In the E11 alloy the etched surface condition was most favourable for low ion release, followed by polishing. Moreover, the influence of proteins was studied in relation to the surface conditions. To determine the difference between the conditions the ratio was calculated (Medium + FBS - pure medium). Here it could be observed, that in most of the cases the addition of FBS increased the ion release (Figure 5 a). The influence of oxygen showed no clear trend. In HBSS it mostly led to a dramatic increase of ion release, whereas in the other solutions the in- or decrease was moderate, with equal observations of increase and decrease (Figure 5 b). In contrast, regarding the release of the alloying elements a reduction of oxygen in most of the cases decreased the release of alloying elements (Figure 5 c)

Figure 5

Corrosion layer analysis

No distinct differences were observable between the corrosion surfaces under normal and reduced oxygen regimes. Therefore only the surfaces of the samples incubated in 21 % O_2 are depicted in the following.

The immersion of the samples in HBSS under cell culture conditions led to an irregular corrosion surface (Figure 6 a). At closer look it exhibited a structured appearance, which was build by a dense conglomerate of very thin platelets (Figure 6 b and c). EDS analysis revealed only Mg, C and O as prevalent elements (Figure 6 d). A standardless EDS quantification showed the atomic percentages of C (3.24), O (90.91) and Mg (5.85).

The addition of 10 % FBS led to a more irregular surface, which was not as closed as the surface by pure HBSS immersion. More holes were observable, presumably due to the evolution of hydrogen, disturbing the formation of a dense layer. By the addition of proteins N and Na as additional elements could be observed (At% - C = 4.54; N = 0.47; O = 90.24; Na = 0.09; Mg = 4.66). This may indicate that a small amount of protein remnants is incorporated in the corrosion layer (Figure 7 a-c).

Immersion in DMEM (Figure 8) led to the formation of a closed layer of crystalline structures (observable by eye as white precipitates). In contrast to HBSS which did not contain calcium, EDS analysis showed the presence of small amounts of calcium in the layer (atomic percent: C = 2.94, O = 94.74, Mg = 2.3 and Ca = 0.02).

When proteins were added to DMEM there was a reduction of crystal formation observable compared to pure DMEM (Figure 9). The corrosion layer close to the sample surface showed two different crystallite orientations. Atomic ratios of the elements were C = 5.34; N = 0.58; O = 90.06; Na = 0.07; Mg = 3.9; P = 0.03; S = 0.01; Ca = 0.01. As this solution is supposed to be the most relevant for physiological corrosion, a cross section of the samples was also analysed. This analysis revealed that the corrosion layer contained the elements Mg, C, O, K, Cl, Na, P, Ca and N (Figure 10 a). Also in this section the crystalline structure could be observed. Moreover, there was a remarkable co-localisation of Ca and P in the vicinity of the sample surface, as determined by EDS mapping (Figure 10 c). The carbon distribution was associated with oxygen (Figure 10 d).

Figure 6

Figure 7

Figure 8

Figure 9

Figure 10

Discussion

One aim of this study was to introduce cell culture conditions as a relevant environment for a more physiological corrosion environment. Cell culture is normally optimized to represent a sustainable environment for proliferating cells. Therefore the standard conditions are comparable to the condition in blood going into the body circuit – a high oxygen saturation, an amount of carbon dioxide in the range of 5-5.5% and body temperature. The used media have the same buffering system as blood, based on $NaHCO_3$ and dissolved CO_2. However, the buffering capacity is dependent on the available amount of $NaHCO_3$. Whereas HBSS contains 350 mg/L, DMEM contains more than tenfold (3700 mg/L). Although this amount determines about 75% of the buffering capacity of the inorganic part of blood, the main other constituents are serum proteins [16], therefore it is necessary to also reflect this part. In our study we decided to add FBS as protein source, well knowing, that other constituents like growth factors, enzymes or antibodies, just to name a few, are present.

The buffering capacity of the medium determined the ion release. It was observed that ion release in DMEM was always lower than in HBSS (Figure 4) and that the addition of proteins always increased the ion release from the materials. This was independent from the surface condition and oxygen regime (Figure 5). This increase may be explained by the stabilization of the pH-value (Figure 2), which was mostly decreased by the addition of proteins, therefore favouring an ongoing release of magnesium from the bulk material. The corrosion of magnesium is highly dependent on the pH (e.g. [6, 17]) and on the composition of the solution [18, 19]. Also the influence of proteins is of importance, which was described for single proteins like albumin [20, 21]. Furthermore, proteins are also interacting with CO_2 by tightly binding both oxygens by acid/base interactions [22]. However, in these studies no cell culture conditions were applied, and the results are contradictory to our study, as corrosion resistance was improved by the addition of proteins [23]. In this study, at least during the first three days, the ion release into the corrosion medium is increased by the addition of proteins. This behaviour indicates a faster initial corrosion. However, long term experiments (14 days

+) showed a higher stability of the samples when immersed in medium + FBS (data not shown). Therefore this initial period of corrosion is worthy of further investigations.

Another study analysed the influence of FBS under cell culture conditions, but the occurrence of carbon (due to the presence of CO_2) was attributed to contamination and therefore not thoroughly discussed {Yamamoto, 2009 #1481}. The general problem of the incomparability of *in vitro* results was recently reviewed [8]. This still is a drawback, as there are many different methodologies (like electrochemistry, gas evolution, immersion tests a.s.o.) available, which give information about the corrosion speed. However, even if appropriate solutions are used there is a common disregard of the buffering capacity. Therefore it would be advisable to introduce the specific environment, even if it requires some efforts. Moreover the comparability to *in vivo* results still is questionable [7] and the ultimate goal would be to directly compare materials in the proposed system with *in vivo* results.

Corrosion products and oxygen

The analysis of the corrosion surface revealed the formation of crystalline precipitates in different forms (Figures 6-9). A comparison with synthetically derived Nesquehonite, $Mg(HCO_3)(OH)\cdot 2H_2O$ or $MgCO_3\cdot 3H_2O$ [24], exhibited high similarities of the crystal structure and preliminary X-ray diffraction studies also confirmed the presence in the corrosion layer (unpublished data). Under atmospheric conditions (0.034% CO_2) the formation of hydromagnesite ($Mg_5(CO_3)_4(OH)_2\cdot 4H_2O$), which was transforming to nesquehonite was observed, followed by pitting corrosion and the formation of brucite [25].

The formation of $MgCO_3$ is hypothesized to be able to retard magnesium corrosion after the formation of a more or less closed layer [11], and to restrict the transport of CO_2 and O_2 to the corrosion interface under atmospheric conditions [25].. In contrast, the corrosion layers observed here and in another study [10] appear to be permeable and this will allow further, but possibly reduced transport of gas and fluid to the surface. This fact may explain the increased magnesium concentration in the extract during the addition of proteins (Figure 4).

Taking the formation of magnesium carbonates into account, this could be an explanation for the drastic reduction in dissolved oxygen (Figure 1). Directly after immersion the formation of hydrogen bubbles is observable, but the incidence of gas formation is reduced or even abandoned over time. Theoretically, this could be due to a direct incorporation of oxygen:

$2\ Mg\ (s) + CO_2 + O_2 \rightarrow 2\ MgCO_3$

Another possible sink for oxygen is the observed formation of calcium phosphates ($Ca_x(PO_4)_x$) in calcium-containing medium (DMEM). Interestingly, the distribution is not homogenous throughout the corrosion layer, but located at the interface of bulk material and corrosion layer (Figure 10). This is also observed *in vivo* in stent applications, where calcification during degradation was found [26-28]. While for stent applications calcification is unwanted, this could be highly relevant for orthopaedic applications.

At the moment we can only hypothesize which mechanism is responsible for the “loss” of dissolved oxygen. However, a possible side effect of this “oxygen drain” may be the induction of low oxygen regimes or even hypoxia, which may attribute to the positive reaction to magnesium degradation. Hypoxic conditions (1% oxygen) in bone positively influence bone formation via the VEGF pathway and by down-regulation of sclerostin [29]. A further observation made in this study was the reduction of pH by low oxygen. This may have an influence on the corrosion speed and will be subject to further studies.

Conclusion

Taking together the experimental and literature data leads to the assumption that the application of cell culture conditions in combination with an appropriately buffered solution including proteins should be a standard for the *in vitro* analysis of magnesium and its alloys. The unravelling of the underlying corrosion mechanisms and of relevant influencing factors can help to optimize *in vitro* test setup to determine magnesium degradation. A study of utmost importance will be the comparison of experimental data from *in vitro* experiments with this setup to data obtained from *in vivo* experiments.

References

1. Witte F. The history of biodegradable magnesium implants: A review. Acta Biomaterialia. 2010;6(5):1680-92.
2. Erbel R, Di Mario C, Bartunek J, Bonnier J, de Bruyne B, Eberli FR et al. Temporary scaffolding of coronary arteries with bioabsorbable magnesium stents: a prospective, non-randomised multicentre trial. Lancet. 2007;369(9576):1869-75.
3. Waksman R, Pakala R, Kuchulakanti PK, Baffour R, Hellinga D, Seabron R et al. Safety and efficacy of bioabsorbable magnesium alloy stents in porcine coronary arteries. Catheterization and Cardiovascular Interventions. 2006;68(4):607-17.
4. Erne P, Schier M, Resink TJ. The road to bioabsorbable stents: reaching clinical reality? Cardiovasc Intervent Radiol. 2006;29(1):11-6.
5. Waksman R, Erbel R, Di Mario C, Bartunek J, de Bruyne B, Eberli FR et al. Early- and Long-Term Intravascular Ultrasound and Angiographic Findings After Bioabsorbable Magnesium Stent Implantation in Human Coronary Arteries. J Am Coll Cardiol Intv. 2009;2(4):312-20. doi:10.1016/j.jcin.2008.09.015.
6. Witte F, Hort N, Vogt C, Cohen S, Willumeit R, Kainer KU et al. Degradable biomaterials based on magnesium corrosion. Current Opinion in Solid State and Materials Science. 2008;12:63-72. doi:10.1016/j.cossms.2009.04.001.
7. Witte F, Fischer J, Nellesen J, Crostack HA, Kaese V, Pisch A et al. In vitro and in vivo corrosion measurements of magnesium alloys. Biomaterials. 2006;27:1013-8.
8. Mueller W-D, Lucia Nascimento M, Lorenzo de Mele MF. Critical discussion of the results from different corrosion studies of Mg and Mg alloys for biomaterial applications. Acta Biomaterialia. 2010;6(5):1749-55.
9. Tie D, Feyerabend F, Hort N, Willumeit R, Hoeche D. XPS Studies of Magnesium Surfaces after Exposure to Dulbecco's Modified Eagle Medium, Hank's Buffered Salt Solution, and Simulated Body Fluid. Advanced Engineering Materials. 2010;12(12):B699-B704.
10. Willumeit R, Fischer J, Feyerabend F, Hort N, Bismayer U, Heidrich S et al. Chemical surface alteration of biodegradable magnesium exposed to corrosion media. Acta Biomaterialia. 2011;7:2704-15.
11. Yamamoto A, Hiromoto S. Effect of inorganic salts, amino acids and proteins on the degradation of pure magnesium in vitro. Materials Science and Engineering: C. 2009;29(5):1559-68.
12. Domm C, Schunke M, Christesen K, Kurz B. Redifferentiation of dedifferentiated bovine articular chondrocytes in alginate culture under low oxygen tension. Osteoarthritis Cartilage. 2002;10(1):13-22.
13. Hansen U, Schunke M, Domm C, Ioannidis N, Hassenpflug J, Gehrke T et al. Combination of reduced oxygen tension and intermittent hydrostatic pressure: a useful tool in articular cartilage tissue engineering. J Biomech. 2001;34(7):941-9.
14. Bassett CA, Herrmann I. Influence of oxygen concentration and mechanical factors on differentiation of connective tissues in vitro. Nature. 1961;190:460-1.
15. Feyerabend F, Fischer J, Holtz J, Witte F, Willumeit R, Drücker H et al. Evaluation of short-term effects of rare earth and other elements used in magnesium alloys on primary cells and cell lines. Acta Biomaterialia. 2010;6(5):1834-42.
16. Ellison G, Straumfjord JV, Jr., Hummel JP. Buffer Capacities of Human Blood and Plasma. Clin Chem. 1958;4(6):452-61.
17. Mueller WD, Nascimento ML, Zeddies M, Córsico M. Magnesium and its Alloys as Degradable Biomaterials. Corrosion Studies Using Potentiodynamic and EIS Electrochemical Techniques. Materials Research. 2007;10(1):5-10.
18. Kirkland NT, Lespagnol J, Birbilis N, Staiger MP. A survey of bio-corrosion rates of magnesium alloys. Corrosion Science. 2010;52(2):287-91.
19. Mueller W-D, Mele MFLd, Nascimento ML, Zeddies M. Degradation of magnesium and its alloys: Dependence on the composition of the synthetic biological media. Journal of Biomedical Materials Research Part A. 2009;90A(2):487-95.

20. Liu C, Xin Y, Tian X, Chu PK. Degradation susceptibility of surgical magnesium alloy in artificial biological fluid containing albumin. Journal of Materials Research. 2007;22(3):1806-14.
21. Rettig R, Virtanen S. Composition of corrosion layers on a magnesium rare-earth alloy in simulated body fluids. Journal of Biomedical Materials Research Part A. 2009;88A(2):359-69.
22. Cundari TR, Wilson AK, Drummond ML, Gonzalez HE, Jorgensen KR, Payne S et al. CO2-Formatics: How Do Proteins Bind Carbon Dioxide? Journal of Chemical Information and Modeling. 2009;49(9):2111-5.
23. Rettig R, Virtanen S. Time-dependent electrochemical characterization of the corrosion of a magnesium rare-earth alloy in simulated body fluids. J Biomed Mater Res A. 2008;85(1):167-75.
24. Kloprogge JT, Martens WN, Nothdurft L, Duong LV, Webb GE. Low temperature synthesis and characterization of nesquehonite. Journal of Materials Science Letters. 2003;22(11):825-9.
25. Jönsson M, Persson D, Thierry D. Corrosion product formation during NaCl induced atmospheric corrosion of magnesium alloy AZ91D. Corrosion Science. 2007;49(3):1540-58.
26. Drynda A, Hassel T, Hoehn R, Perz A, Bach F-W, Peuster M. Development and biocompatibility of a novel corrodible fluoride-coated magnesium-calcium alloy with improved degradation kinetics and adequate mechanical properties for cardiovascular applications. Journal of Biomedical Materials Research Part A. 2010;93A(2):763-75.
27. Drynda A, Deinet N, Braun N, Peuster M. Rare earth metals used in biodegradable magnesium-based stents do not interfere with proliferation of smooth muscle cells but do induce the upregulation of inflammatory genes. Journal of Biomedical Materials Research Part A. 2009;91A(2):360-9.
28. Hermawan H, Dubé D, Mantovani D. Developments in metallic biodegradable stents. Acta Biomaterialia. 2010;6(5):1693-7.
29. Genetos DC, Toupadakis CA, Raheja LF, Wong A, Papanicolaou SE, Fyhrie DP et al. Hypoxia decreases sclerostin expression and increases Wnt signaling in osteoblasts. Journal of Cellular Biochemistry. 2010;110(2):457-67.

Figure captions

Figure 11: Reduction of oxygen tension by magnesium corrosion under different environmental oxygen tensions (5 and 21%). Absolute reduction in HBSS (1a) and DMEM (1c) and values given as percentage (1b: HBSS and 1d: DMEM).

Figure 12: Differences in the averages of the online pH measurements compared for the addition of proteins (a) and between 5 and 21% oxygen. Ero= arc erosion; pol= electro polished; etch=etched; FBS=addition of proteins (10% fetal bovine serum)

Figure 13: Increase of osmolality as function of immersion time.

Figure 14: Ion release from polished samples of pure Mg, WE43 and E11 as a function of time, oxygen content and protein addition.

Figure 15: Dependency of magnesium release on the addition of proteins (a) and oxygen tension (b). In nearly all cases the addition of proteins increases the ion release, whereas for reduced oxygen no clear trend could be observed. In c) the influence of oxygen on the release of alloying elements is shown.

Figure 16: Corrosion surface visualization of samples immersed in HBSS by SEM, detector SE2, accelerating voltage 5kV (a-c) and elemental distribution determined by EDX (d).

Figure 17: Aspects of corrosion surface after immersion in HBSS + 10 % FBS (a + b). The addition of proteins leads to a more irregular corrosion layer and to the introduction of the elements N and Na (c).

Figure 18: Corrosion layer after immersion in DMEM. A close layer of crystallites is formed on the surface (a + b). Traces of Calcium can be found in the layer (c).

Figure 19: Surface analysis of magnesium samples after immersion in DMEM + 10 % FBS. Crystal formation is reduced (a). The corrosion surface (b) is determined by two different crystal orientations (c and d). E9 shows the EDS analysis revealing the presence of

Figure 20: Cross section of the corrosion of a magnesium sample immersed in DMEM + FBS. A) shows the EDS analysis of elements found in the corrosion cross section; in b) the plain image of the cross section is shown (BSE, 20 keV); c) displays the perfect colocalisation of calcium and phosphorous analysed by EDS-mapping and d) shows the overlay of oxygen (blue) and carbon (red), also showing a high degree of overlapping.

Table 1: Composition of the used corrosion media in wt% and molarity. It has to be noted that DMEM already contains a certain amount of magnesium (highlighted in grey).

	HBSS		DMEM	
Ingredient	mg/L	mM	mg/L	mM
Amino Acids				
Glycine			30	0.400
L-Alanyl-L-Glutamine			862	3.97
L-Arginine hydrochloride			84	0.398
L-Cystine 2HCl			63	0.201
L-Histidine hydrochloride-H2O			42	0.200
L-Isoleucine			105	0.802
L-Leucine			105	0.802
L-Lysine hydrochloride			146	0.798
L-Methionine			30	0.201
L-Phenylalanine			66	0.400
L-Serine			42	0.400
L-Threonine			95	0.798
L-Tryptophan			16	0.0784
L-Tyrosine			72	0.398
L-Valine			94	0.803
Vitamins				
Choline chloride			4	0.0286
D-Calcium pantothenate			4	0.00839
Folic Acid			4	0.00907
i-Inositol			7.2	0.0400
Niacinamide			4	0.0328
Pyridoxine hydrochloride			4	0.0196
Riboflavin			0.4	0.00106
Thiamine hydrochloride			4	0.0119
Inorganic Salts				
Calcium Chloride (CaCl2-2H2O)			264	1.80
Ferric Nitrate (Fe(NO3)3"9H2O)			0.1	0.000248
Hydrochloric acid (HCl)				
Magnesium Sulfate (MgSO4-7H2O)			200	0.813
Potassium Chloride (KCl)	400	5.33	400	5.33
Potassium Phosphate monobasic (KH2PO4)	60	0.441		
Sodium Bicarbonate (NaHCO3)	350	4.17	3700	44.05
Sodium Chloride (NaCl)	8000	137.93	6400	110.34
Sodium Phosphate monobasic (NaH2PO4-2H2O)			141	0.916
Sodium Phosphate dibasic (Na2HPO4) anhydrous	48	0.338		
Other Components				
D-Glucose (Dextrose)	1000	5.56	4500	25.00
Phenol Red			15	0.0399
Sodium Pyruvate			110	1.000

Table 2: Average oxygen tension determined in the different solutions. Given are means and standard deviation of 4 measurements each (up to 16000 measuring points per sample). The oxygen consumption in 21% oxygen was higher in all cases than at a partial pressure of 5%. The addition of magnesium increased the standard deviation in all cases, indicating higher sample variability.

Medium	**5 % O_2**	**21 % O_2**
HBSS	4.644 ± 0.185	21.400 ± 0.271
HBSS + Mg	3.300 ± 0.450	14.482 ± 1.022
HBSS + FBS	4.456 ± 0.132	21.136 ± 0.162
HBSS + FBS + Mg	3.506 ± 0.541	13.974 ± 1.553
DMEM	5.148 ± 0.114	22.021 ± 0.156
DMEM + Mg	3.079 ± 0.525	11.880 ± 2.415
DMEM + FBS	5.028 ± 0.151	22.085 ± 0.160
DMEM + FBS + Mg	3.415 ± 0.390	10.862 ± 2.541

Table 3: Cumulative release over three days of magnesium and alloying elements determined by ICP-OES. * denominates samples which were disintegrated during the immersion period.

Figure 1a
Click here to download high resolution image

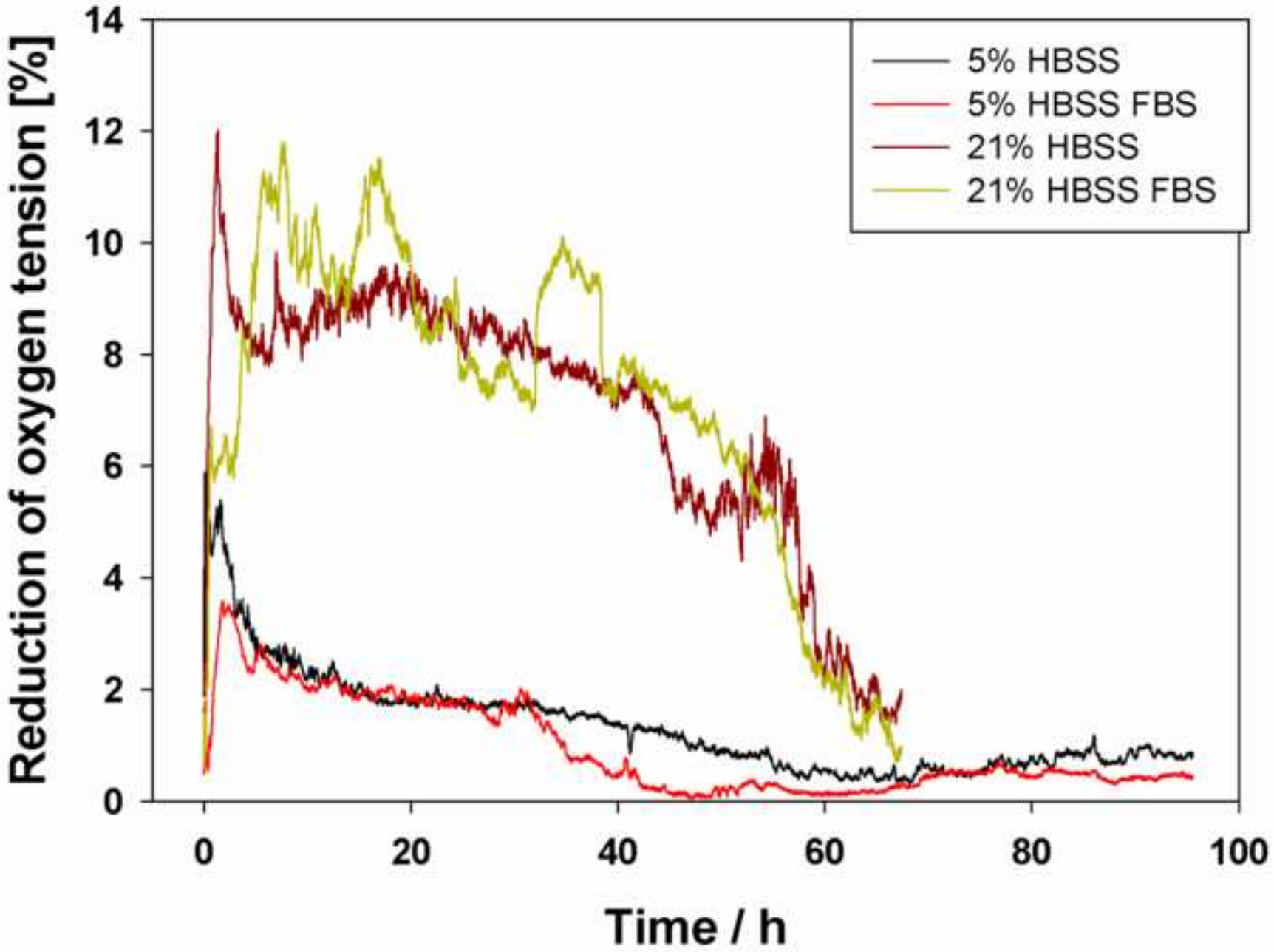

Figure 1b
Click here to download Figure: Figure 1b.EPS

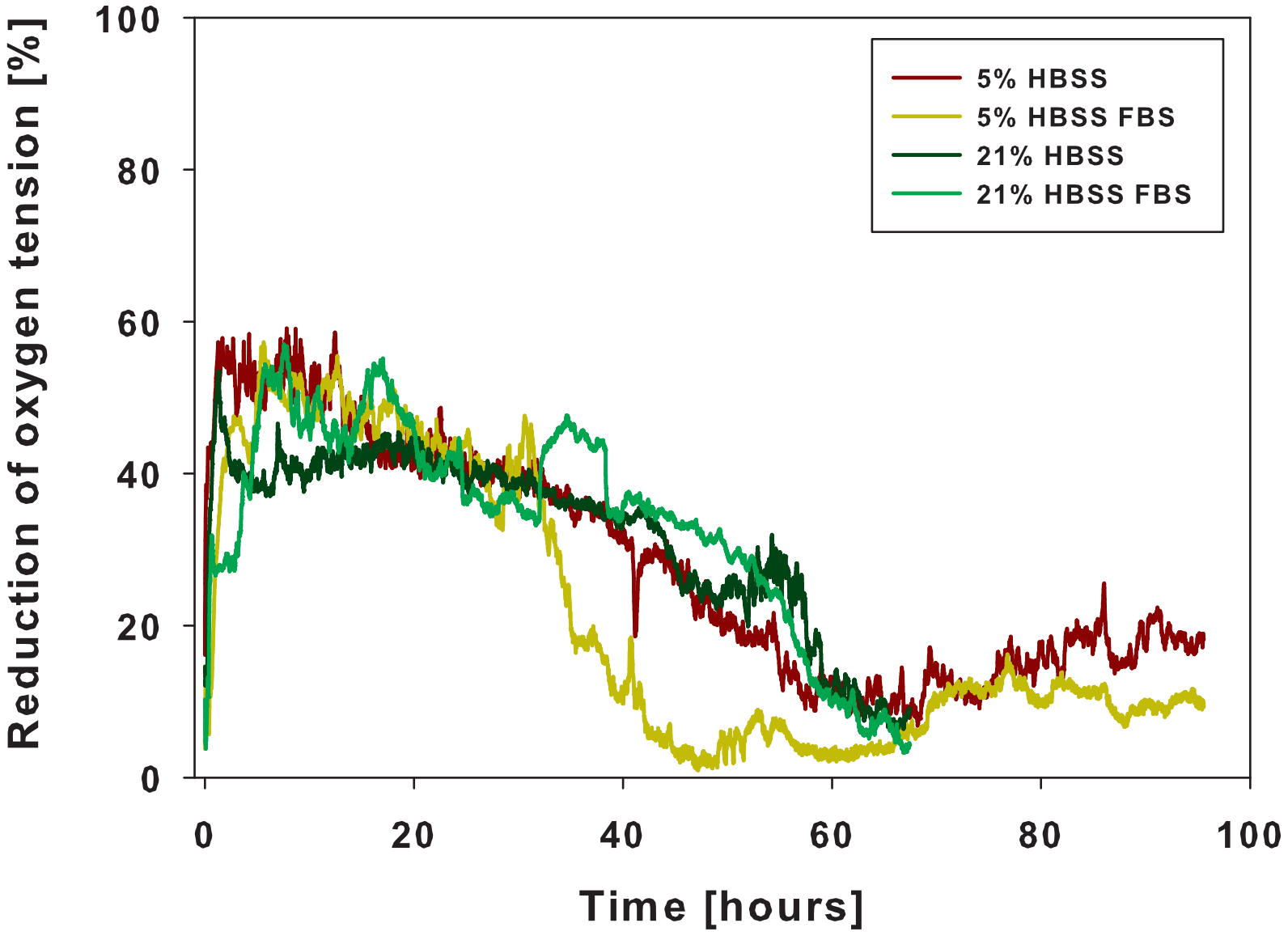

Figure 1c

Click here to download high resolution image

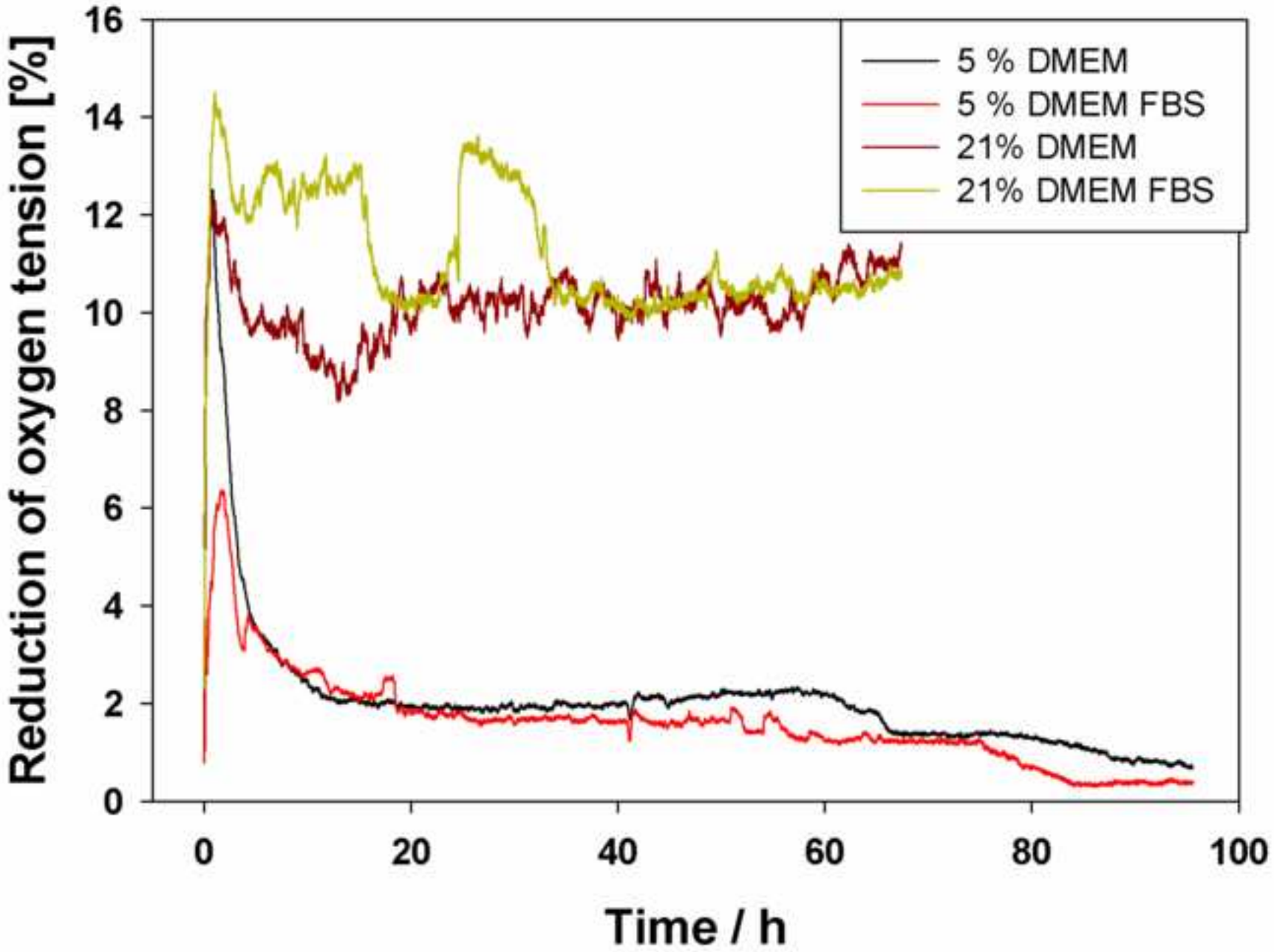

Figure 1d
Click here to download Figure: Figure 1d.EPS

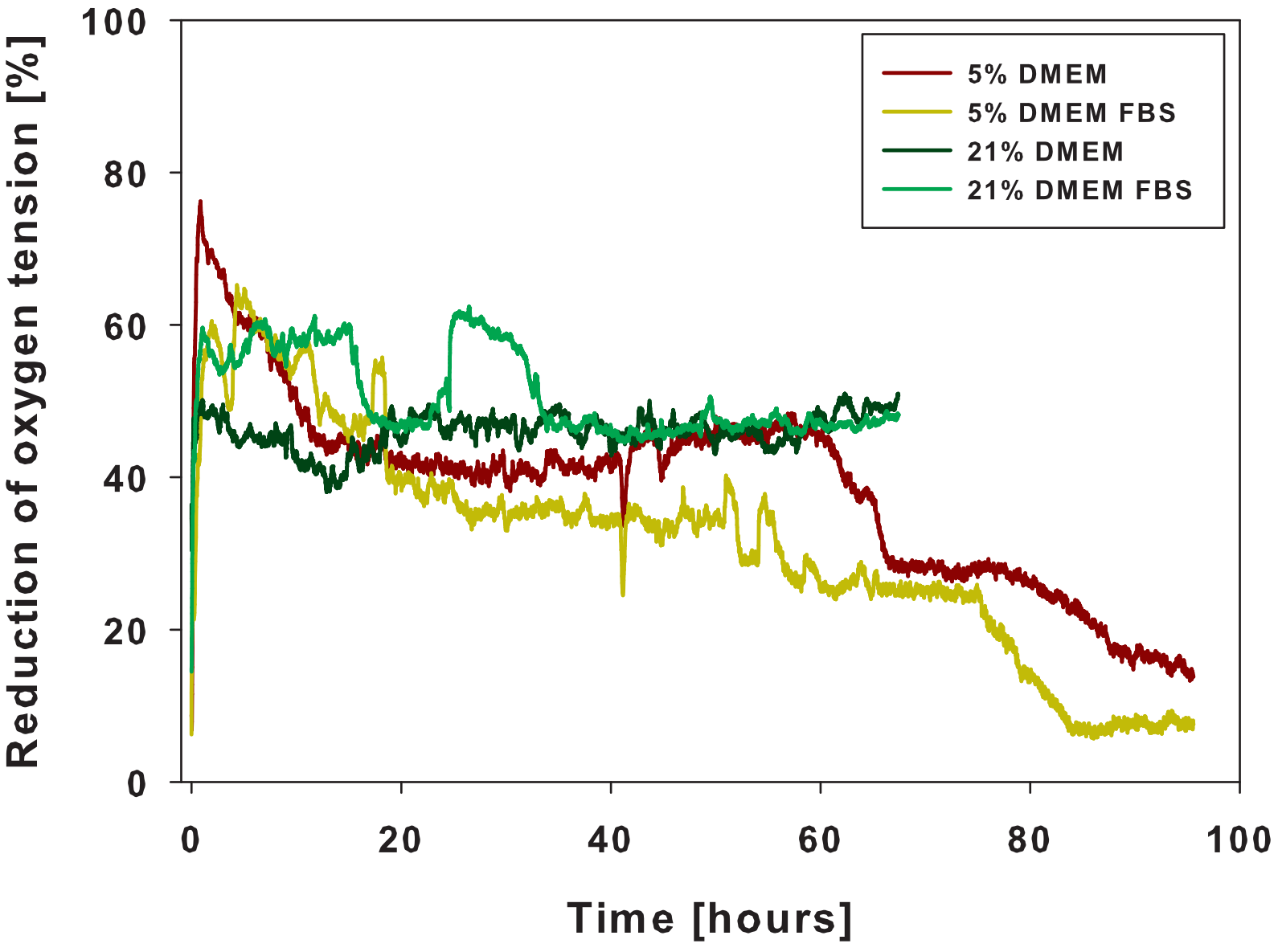

Figure 2a
Click here to download Figure: Figure 2a.EPS

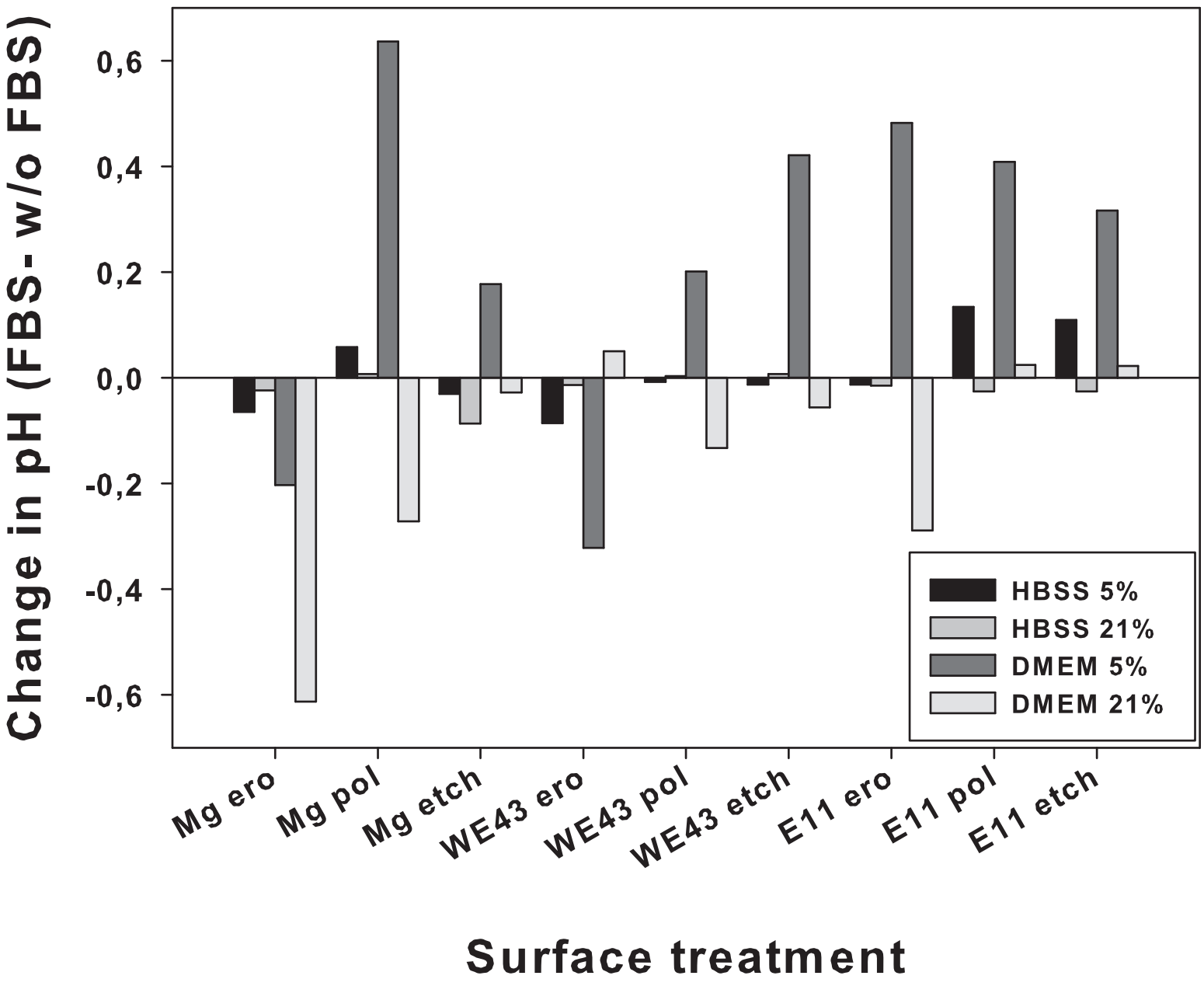

Figure 2b
Click here to download Figure: Figure 2b.EPS

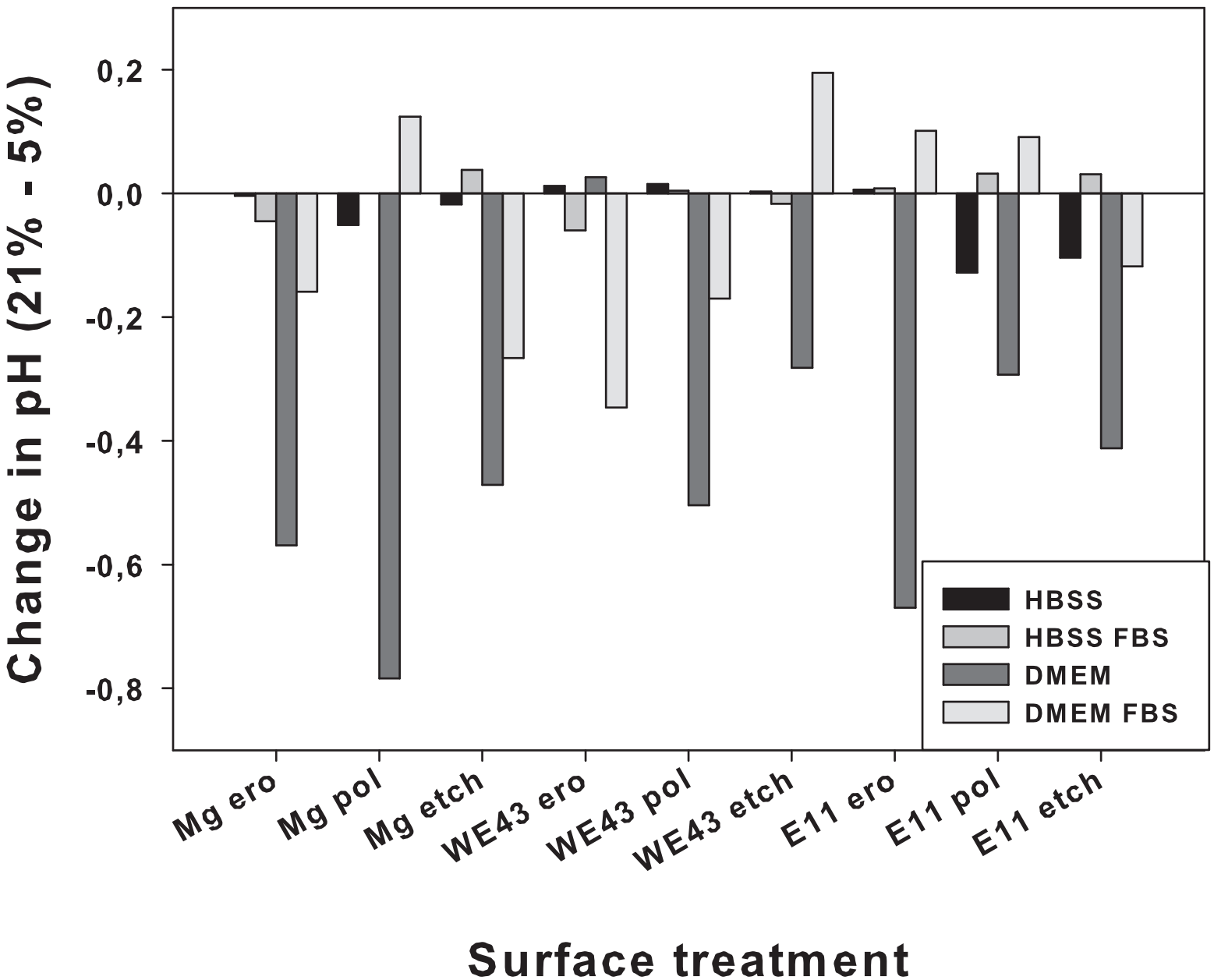

Figure 3a
Click here to download Figure: Figure 3a.EPS

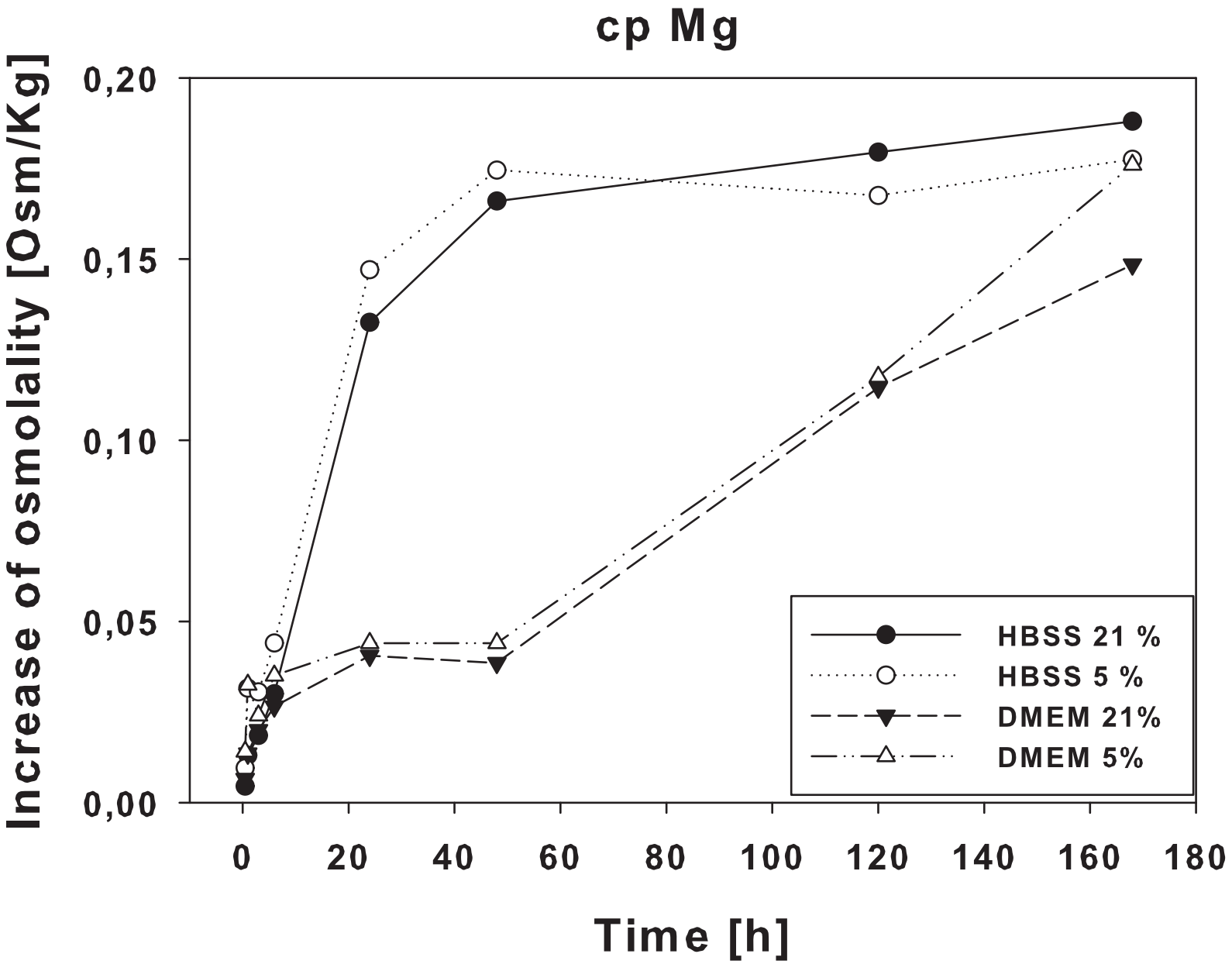

Figure 3b
Click here to download Figure: Figure 3b.EPS

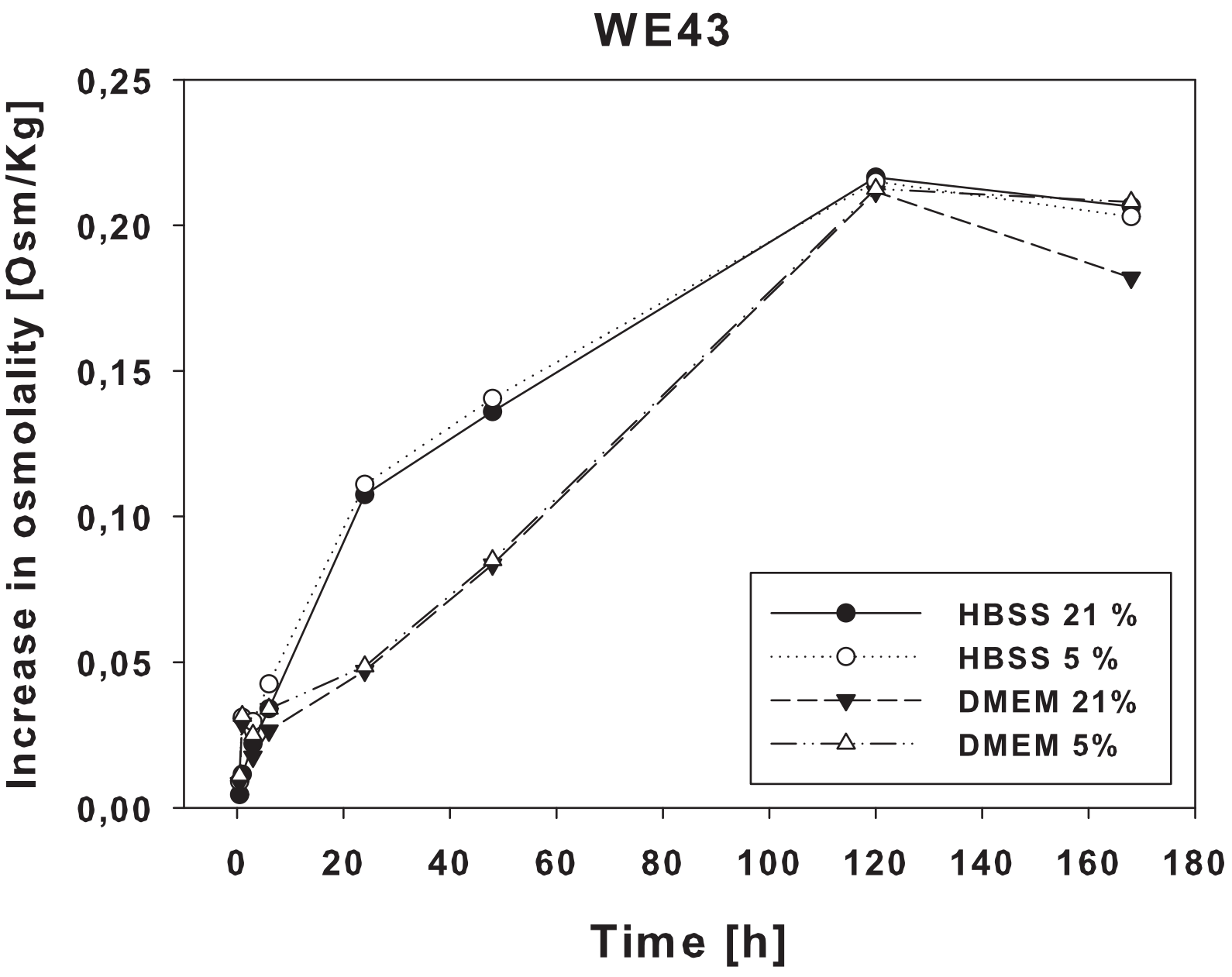

Figure 3c
Click here to download Figure: Figure3c.EPS

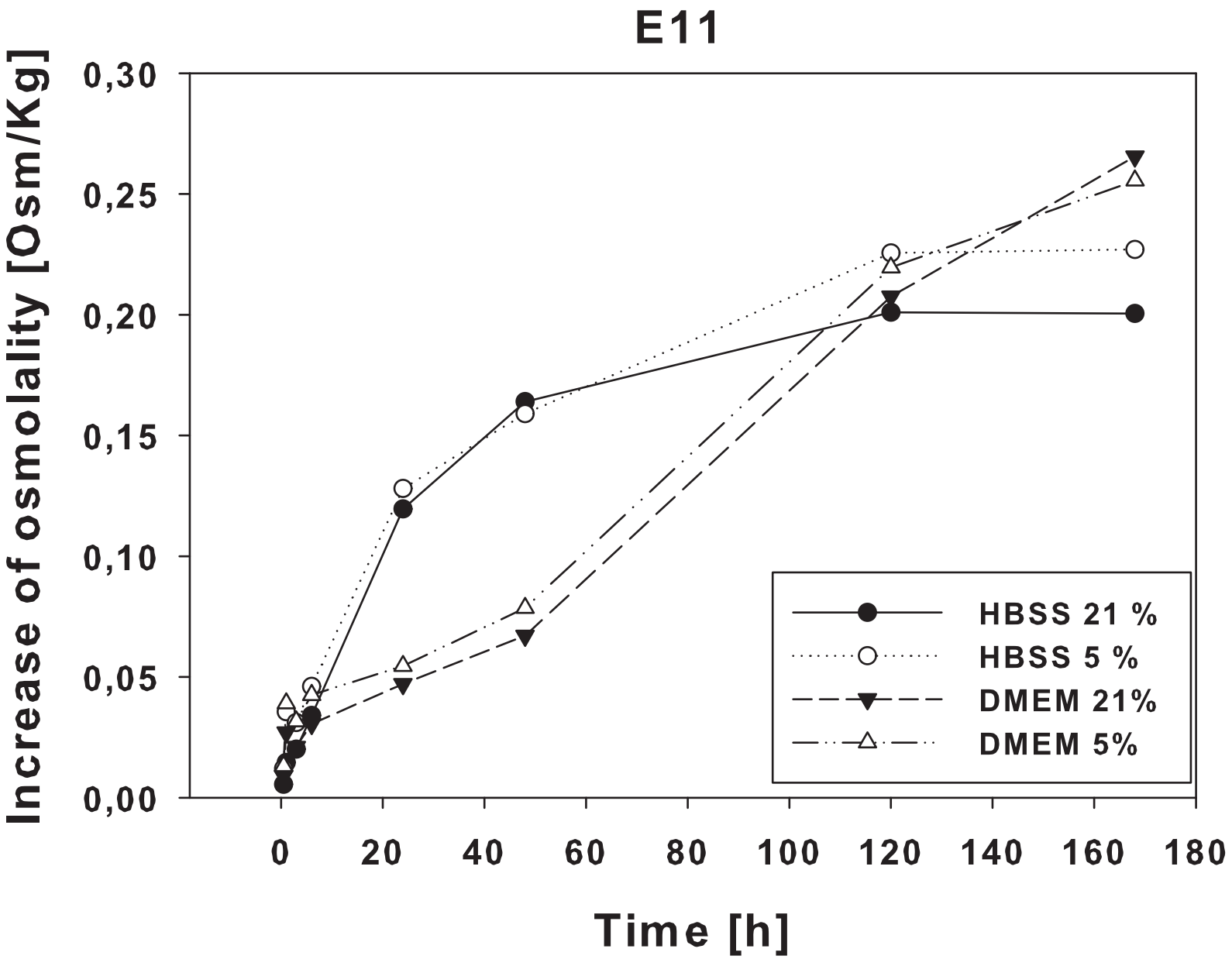

Figure 4a

Click here to download Figure: Figure 4a.EPS

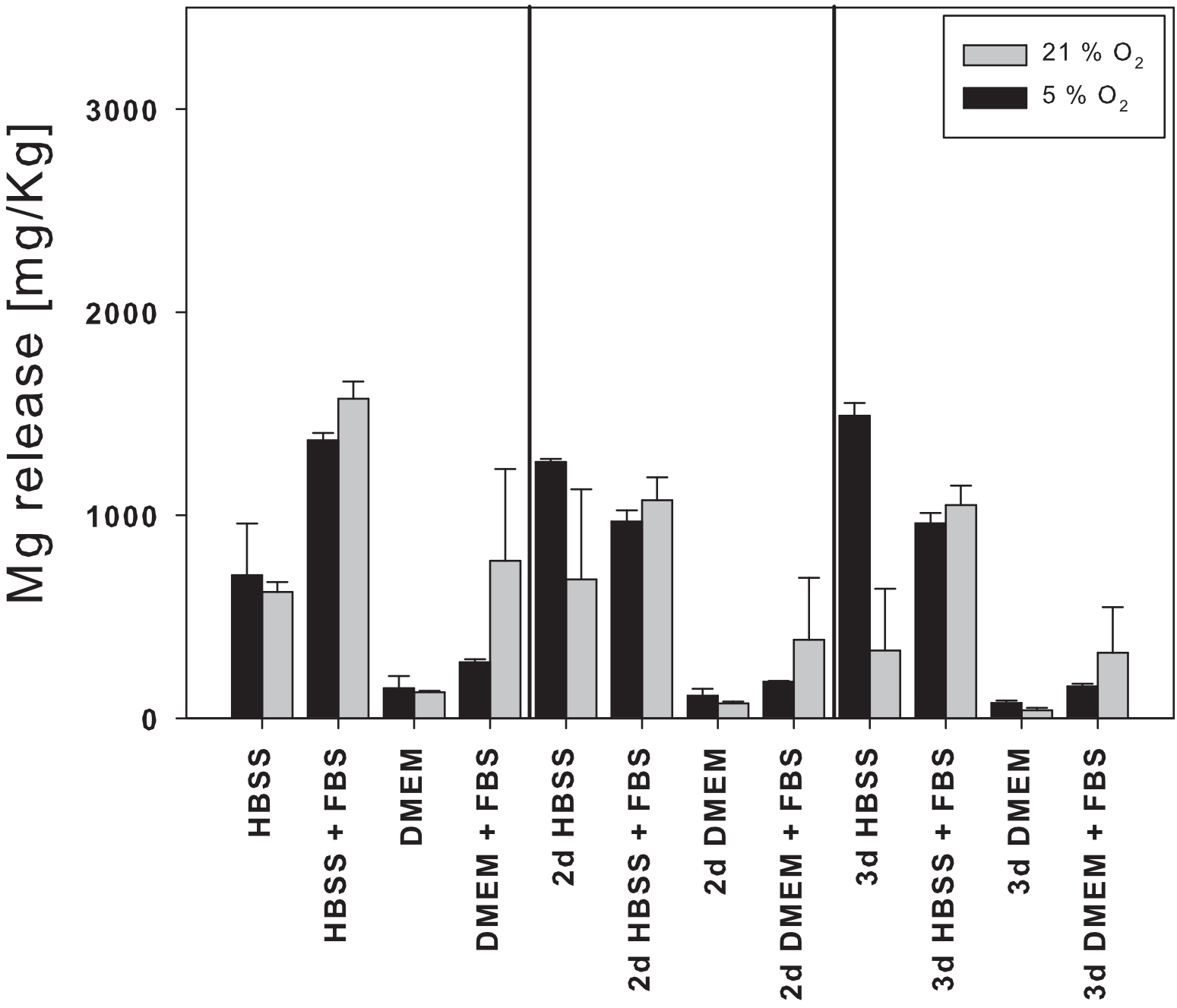

Figure 4b

Click here to download Figure: Figure 4b.doc

WE43

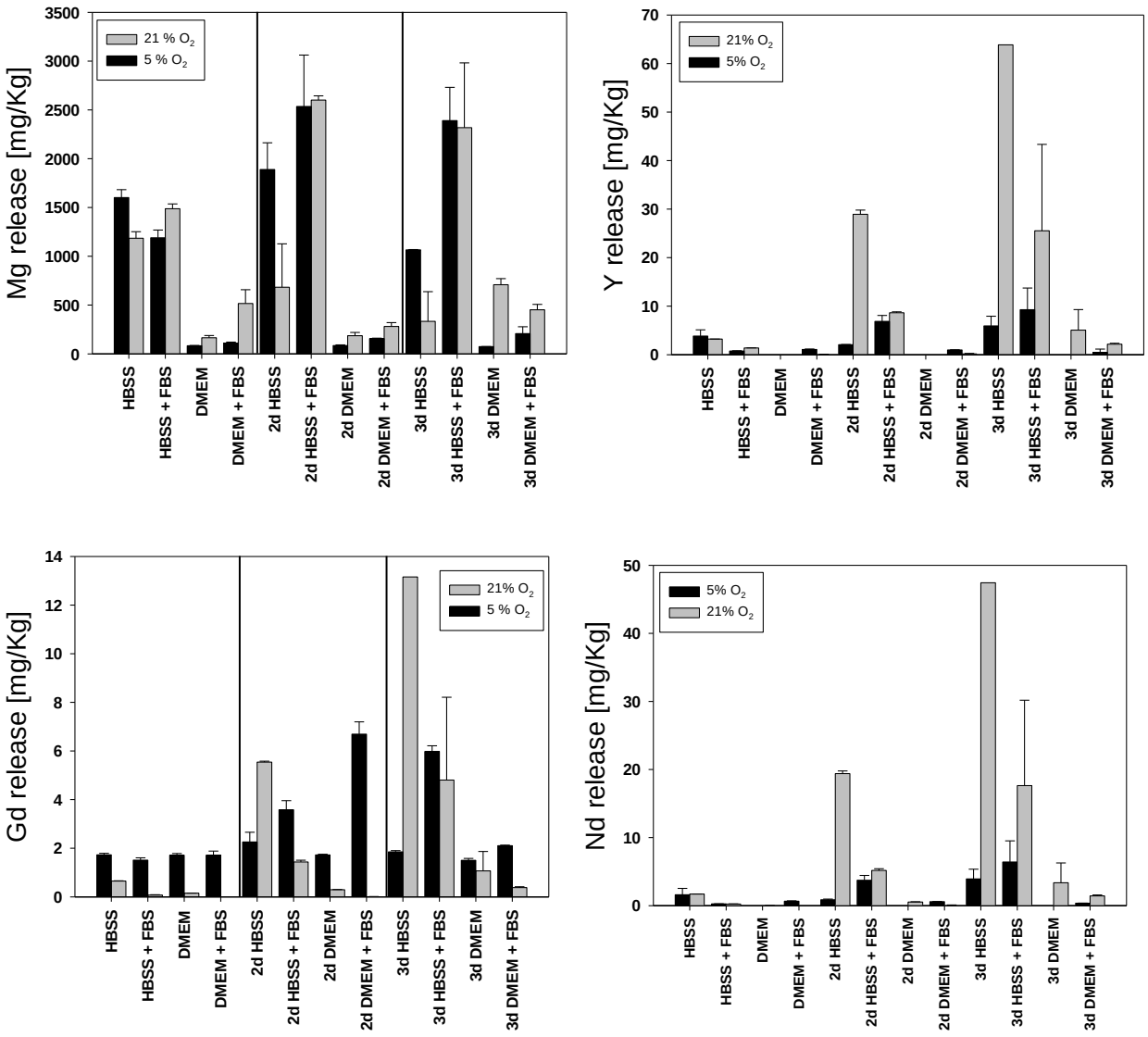

Figure 4c

Click here to download Figure: Figure 4c.doc

E11

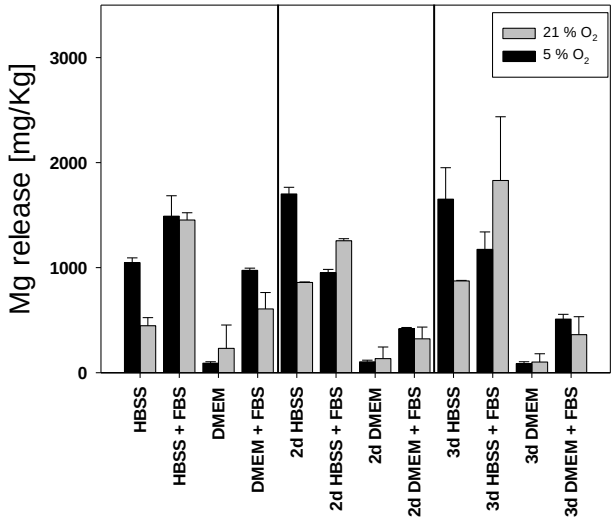

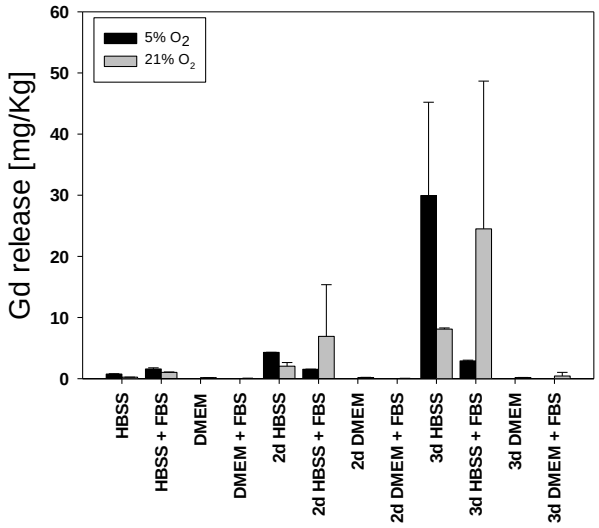

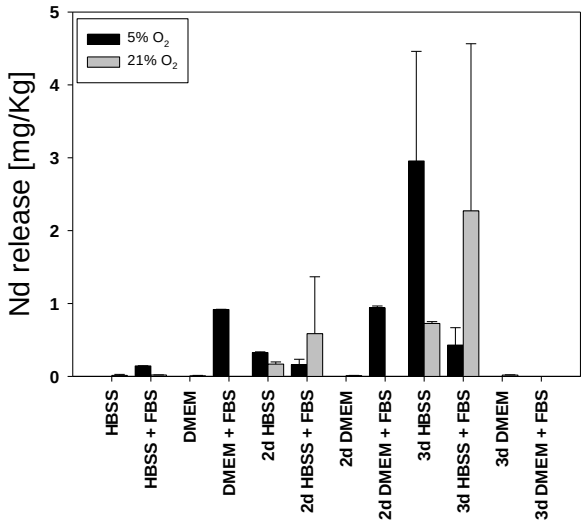

Figure 5a

Click here to download Figure: Figure 5a.EPS

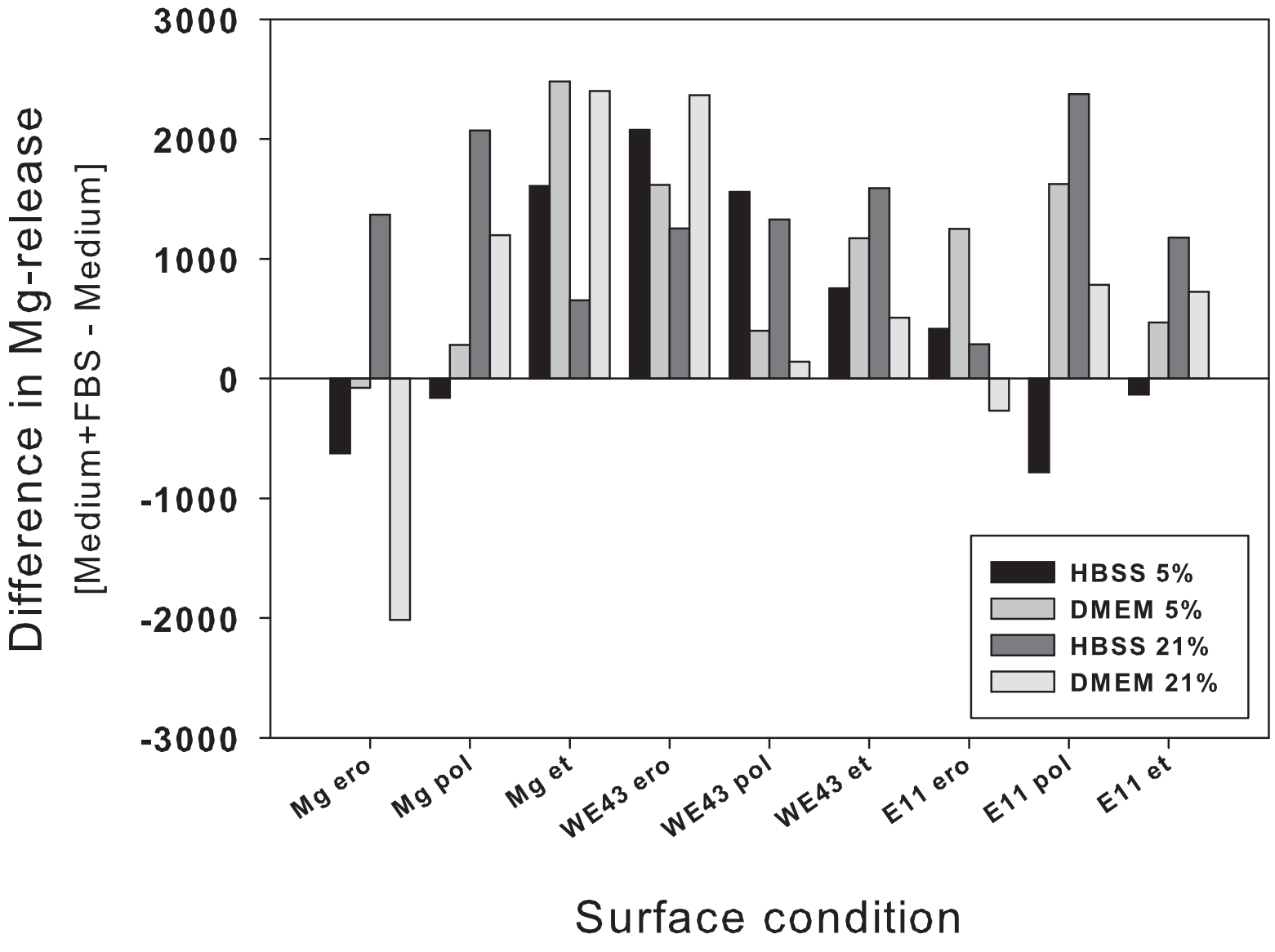

Figure 5b
Click here to download Figure: Figure 5b.EPS

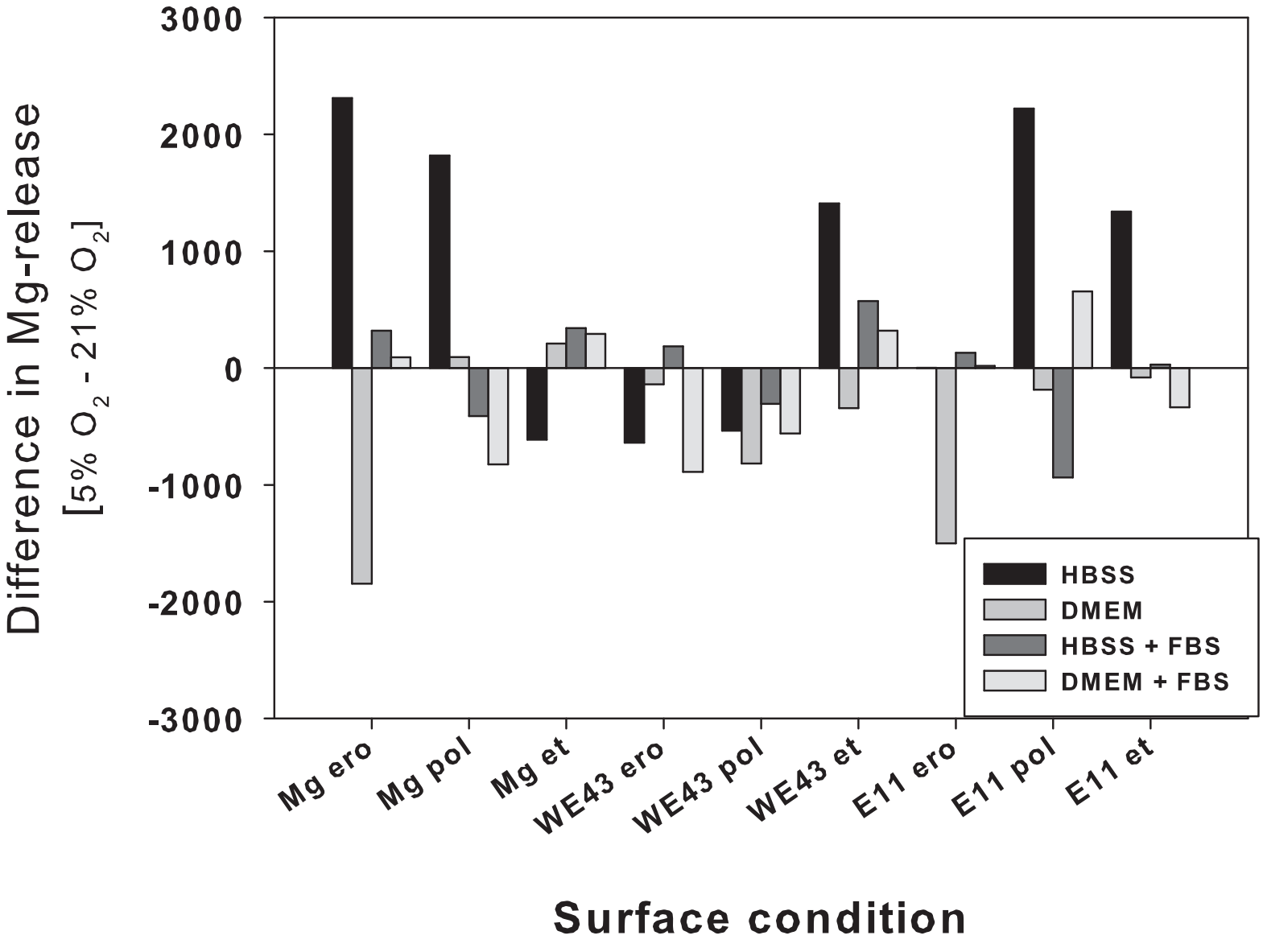

Figure 5c
Click here to download Figure: Figure 5c.EPS

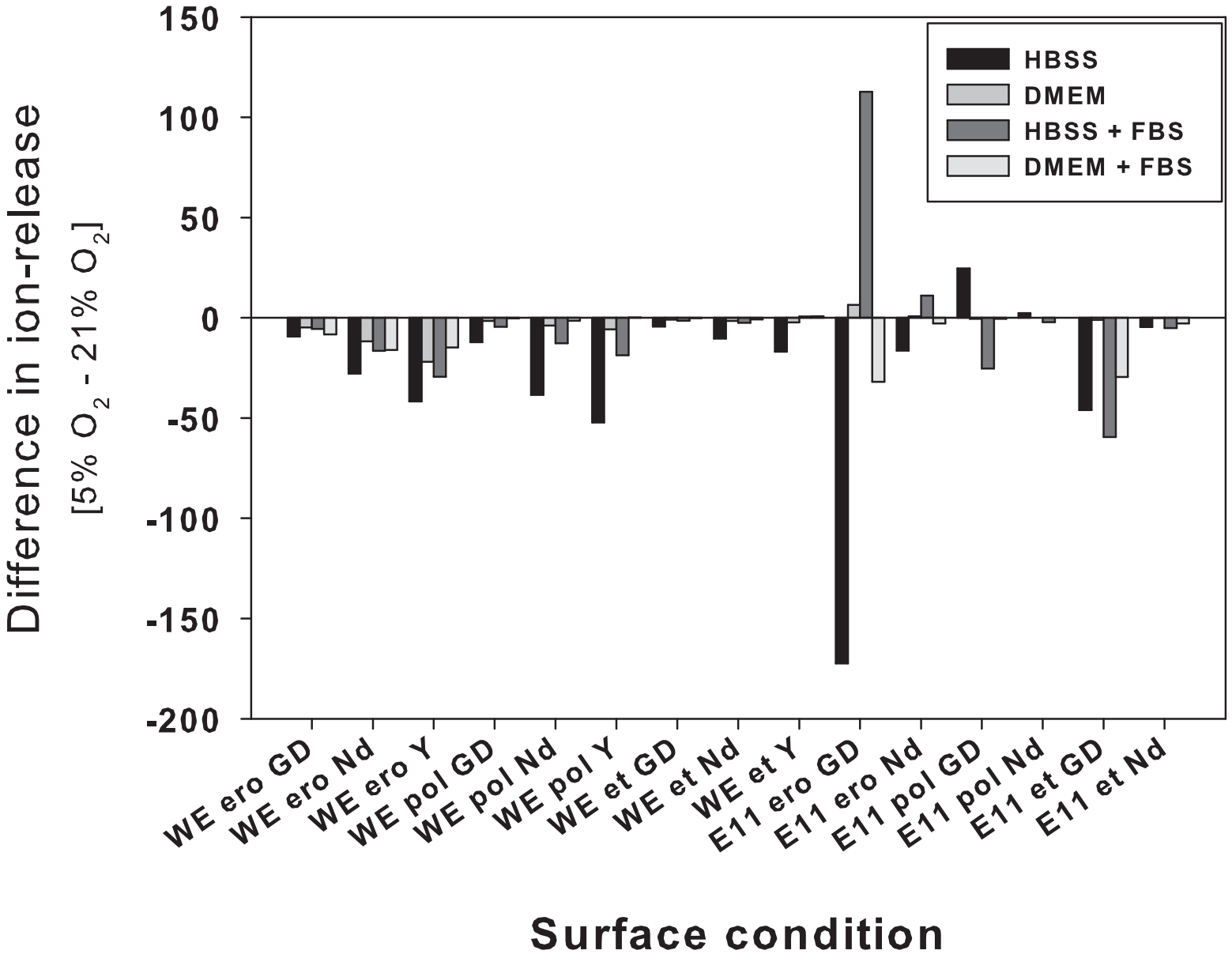

Figure 6

Click here to download Figure: Figure 6.doc

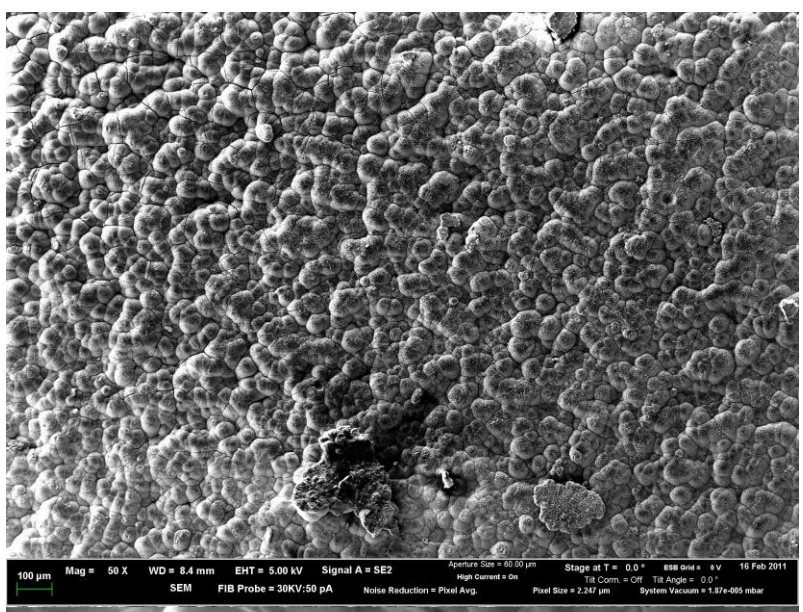

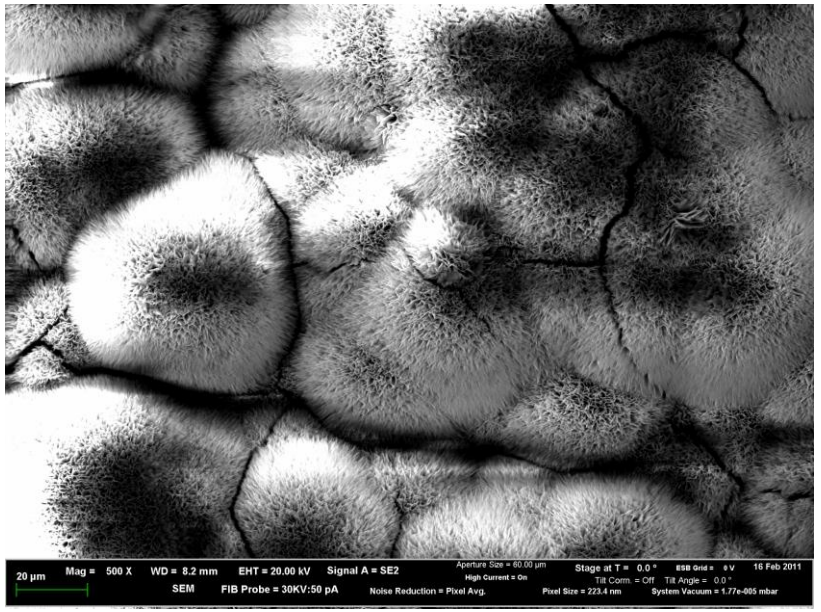

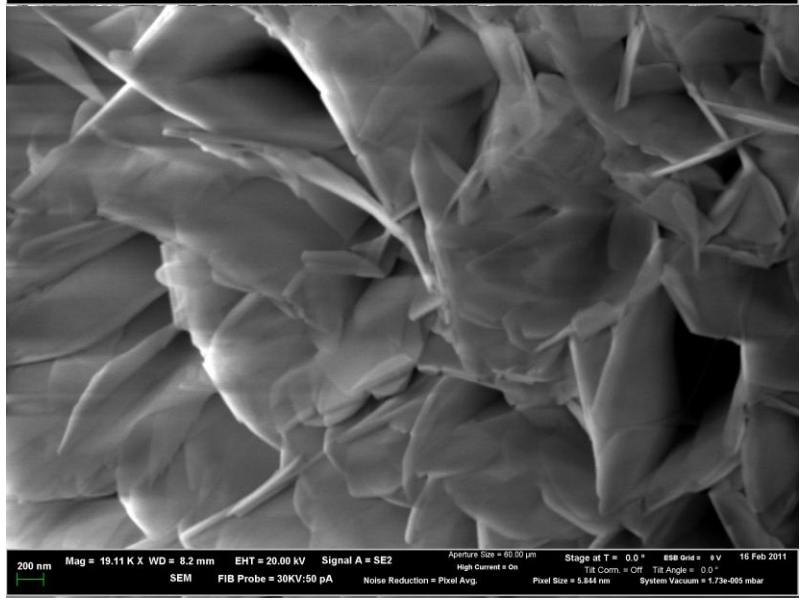

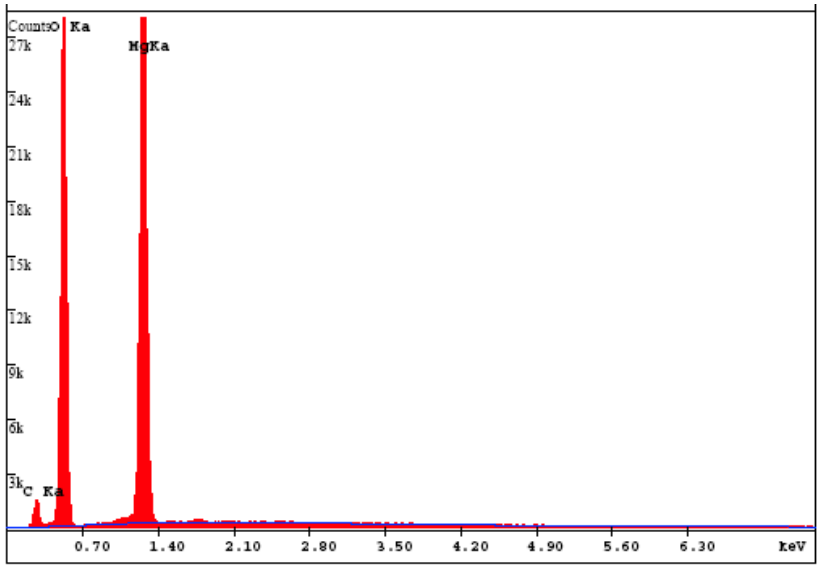

Figure 7

Click here to download Figure: Figure 7.doc

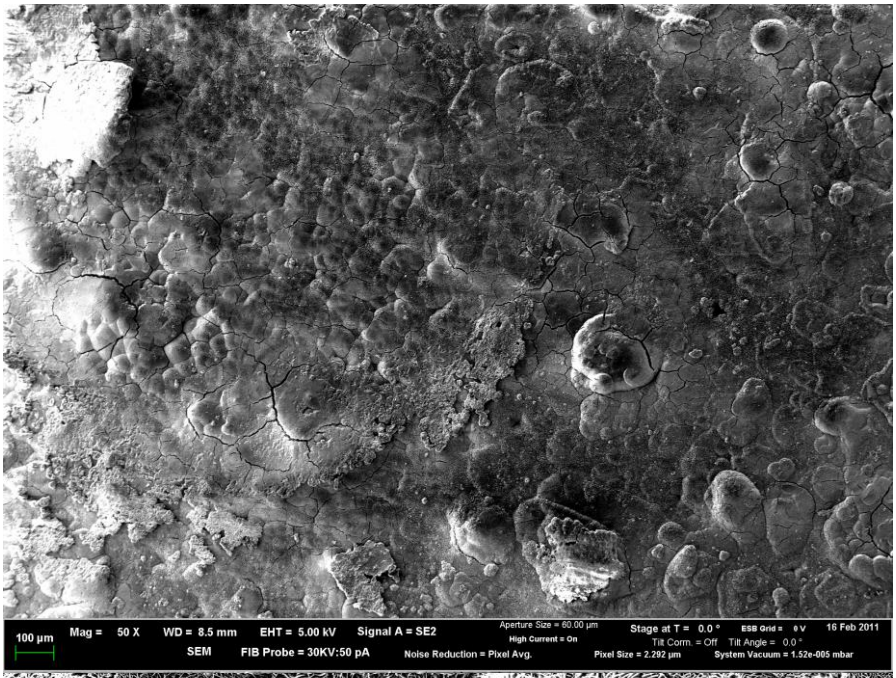

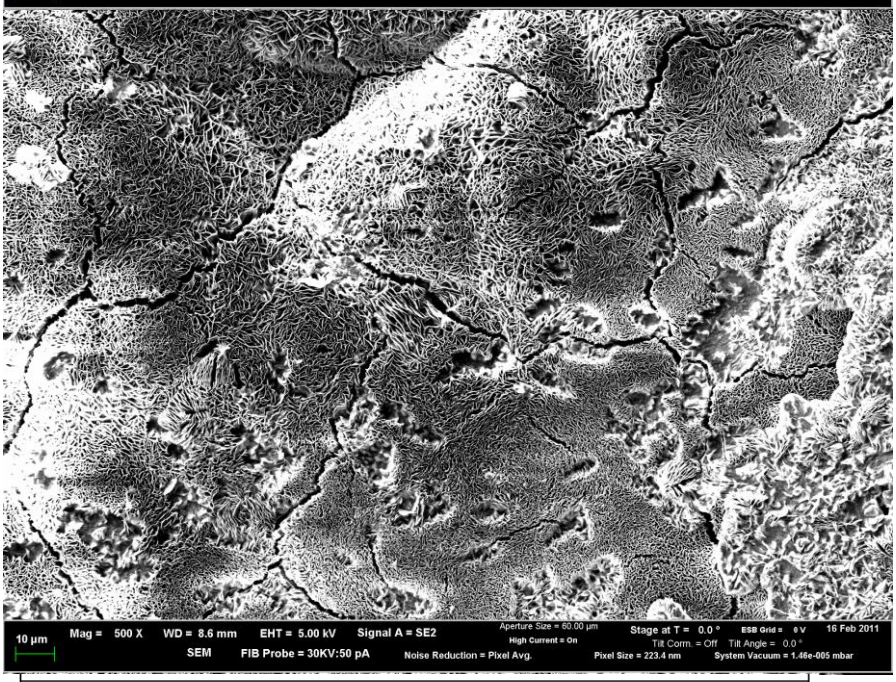

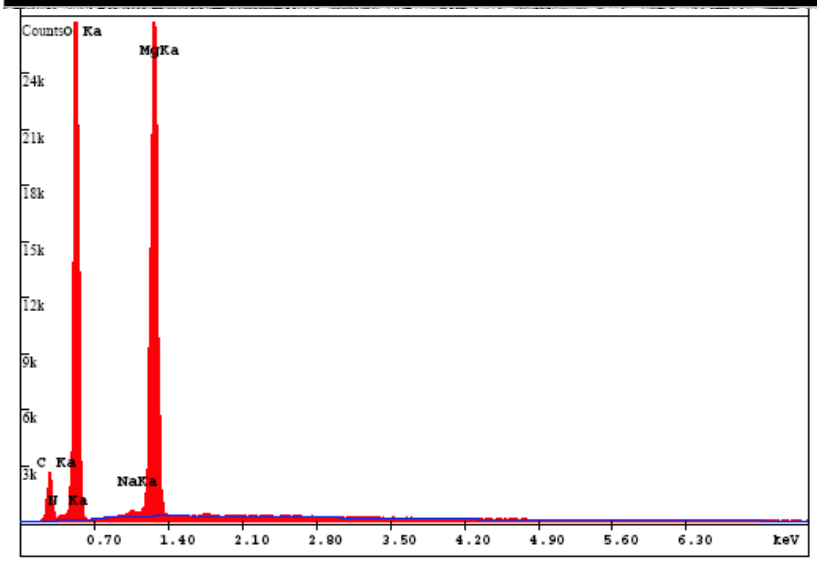

Figure 8

Click here to download Figure: Figure 8.doc

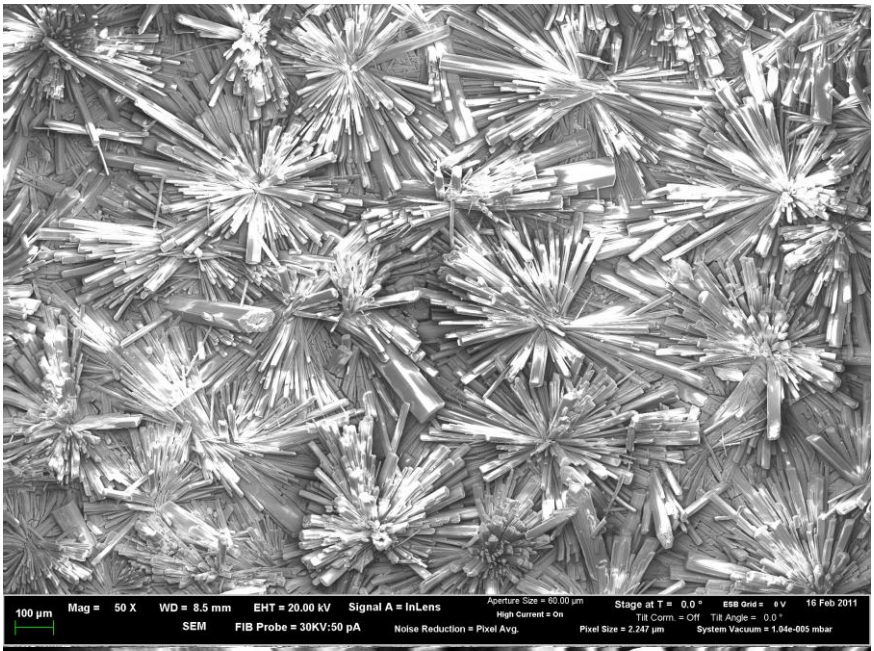

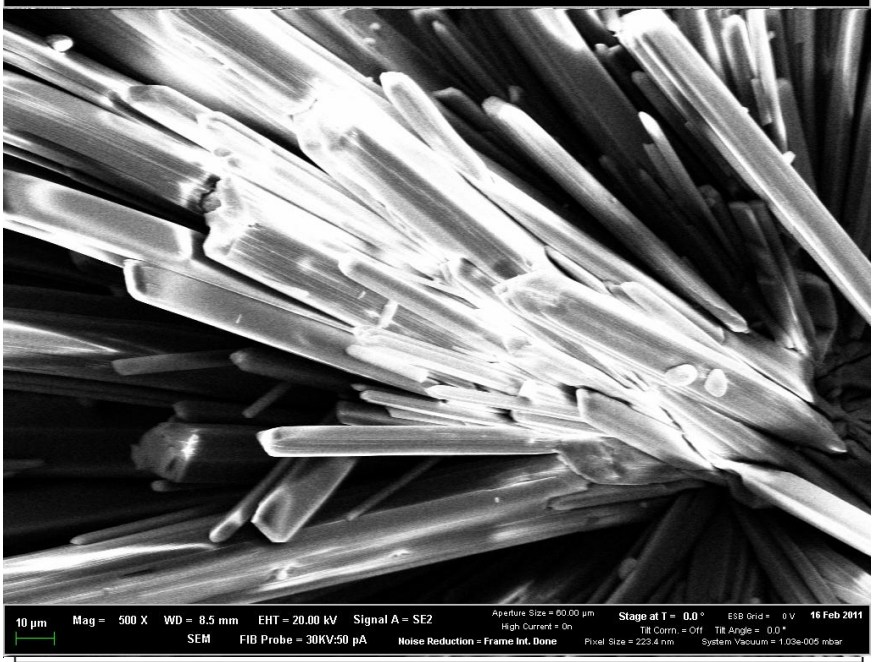

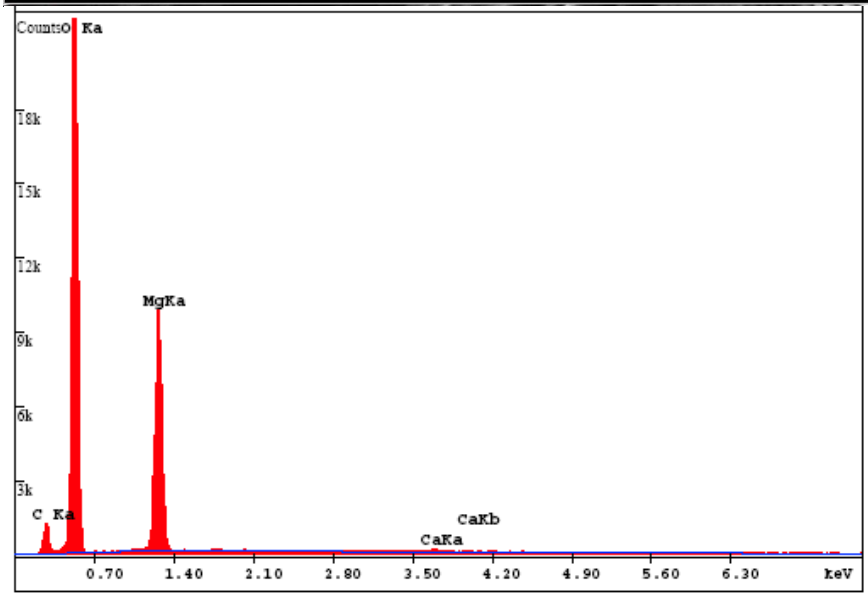

Figure 9

Click here to download Figure: Figure 9.doc

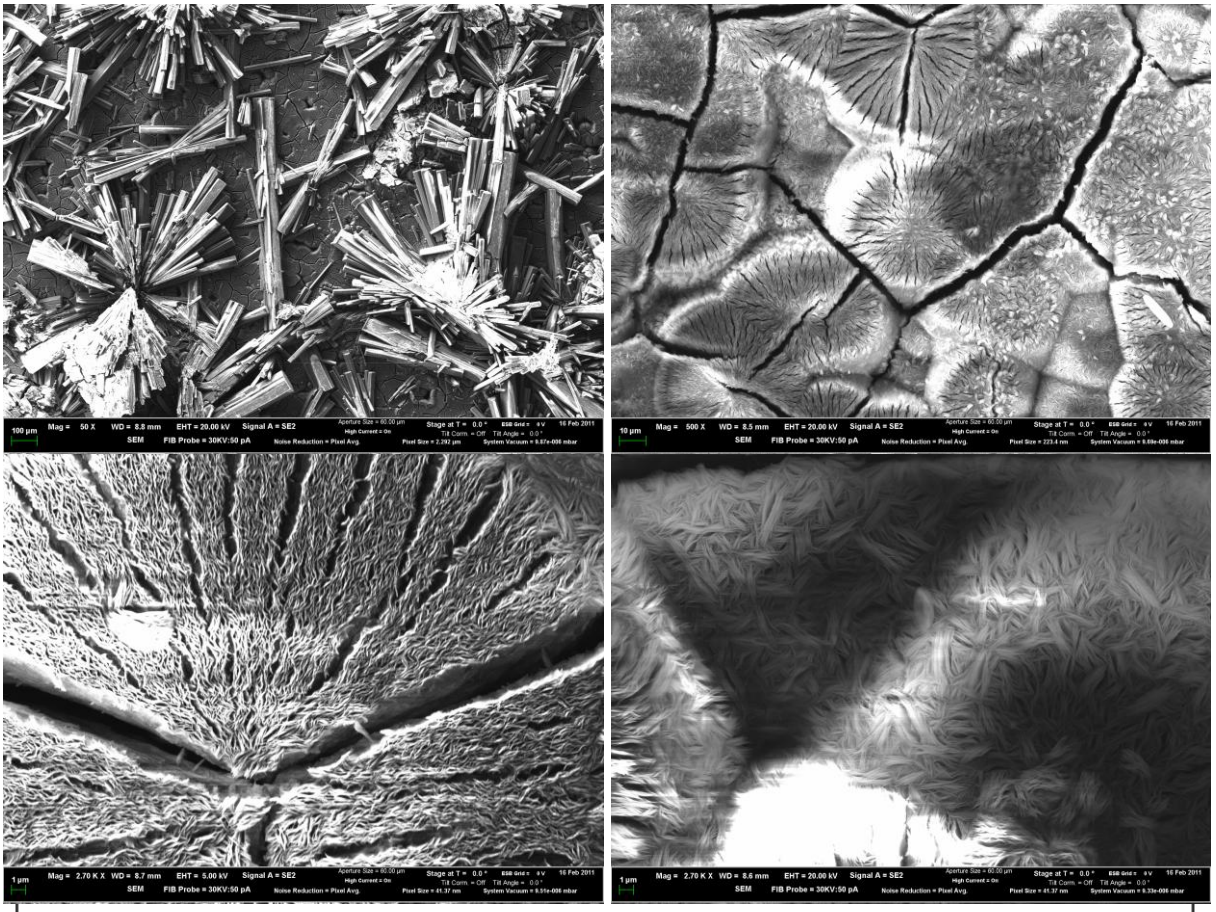

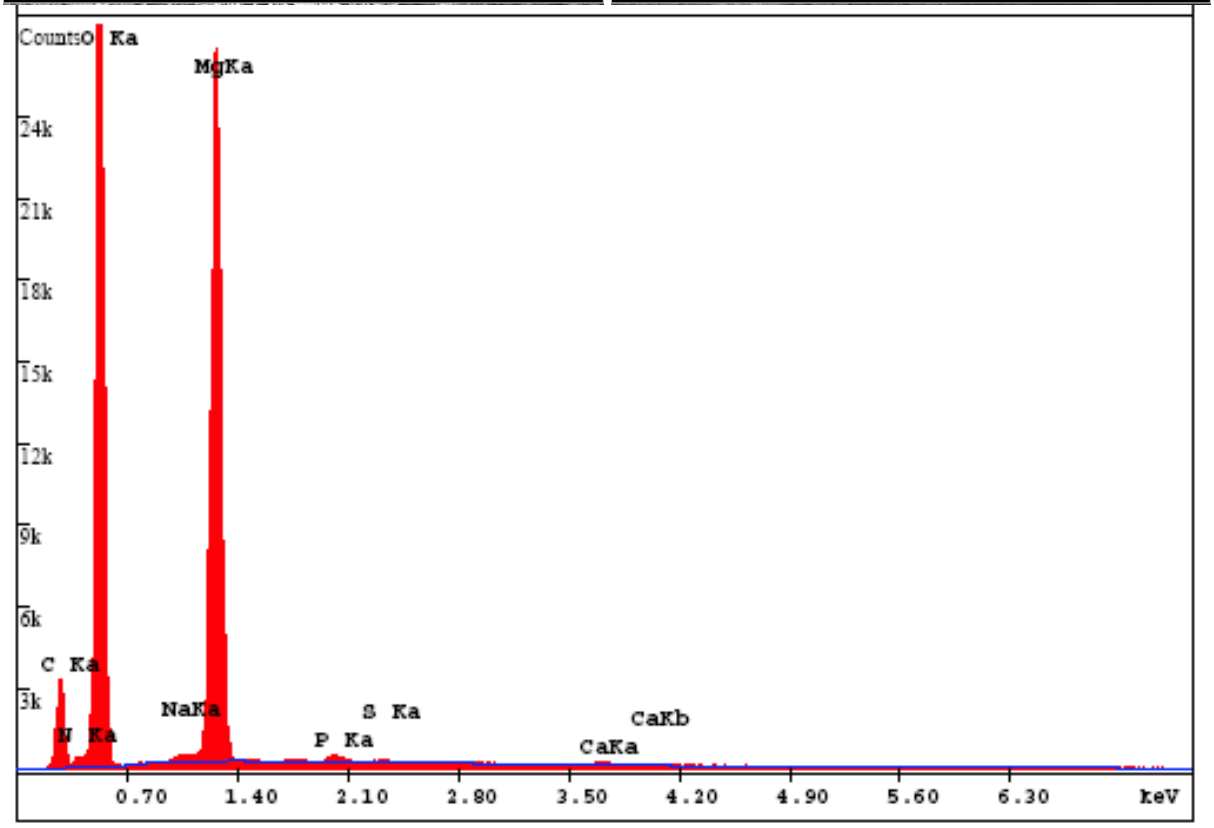

Figure 10

Click here to download Figure: Figure 10.doc

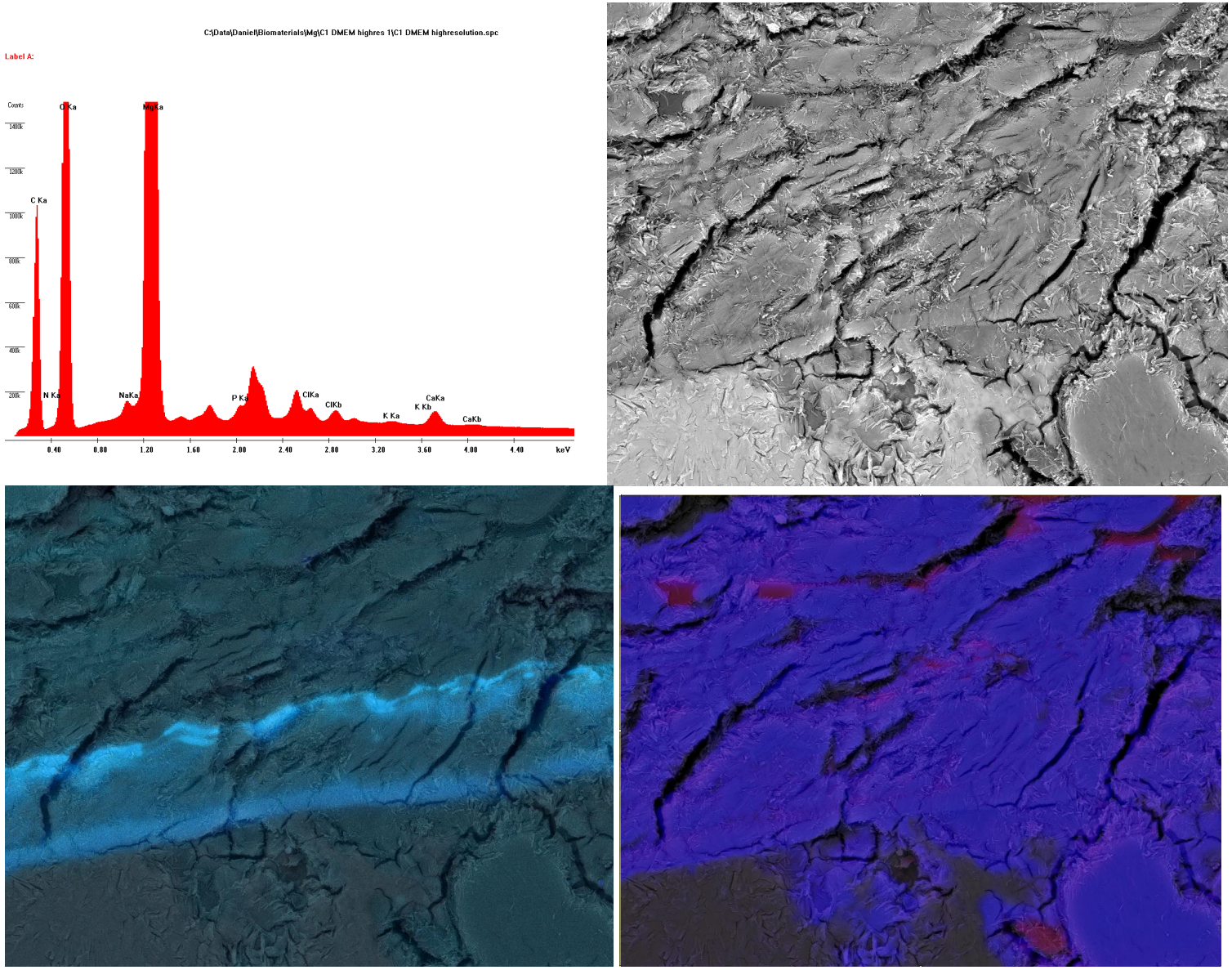

Table

Click here to download Table: Table 3 cumulative release.doc

Table 3: Cumulative release over three days of magnesium and alloying elements determined by ICP-OES. * denominates samples which were disintegrated during the immersion period.

Sample	Surface condition	Cumulative release of magnesium [mg/kg]							
		5 % oxygen				21 % oxygen			
		HBSS	DMEM	HBSS+FBS	DMEM+FBS	HBSS	DMEM	HBSS+FBS	DMEM+FBS
Mg	Eroded	4528,35 ± 115,60	906,07 ± 237,46	3902,97 ± 118,50	828,82 ± 132,47	2216,69 ± 53,37	2752,58 ± 696,22	3582,78 ± 161,57	737,06 ± 202,25
	Polished	3457,36 ± 329,75	332,73 ± 107,41	3297,26 ± 41,29	611,62 ± 0,43	1638,11 ± 92,11	239,57 ± 27,91	3709,45 ± 293,02	1436,22 ± 984,29
	Etched	2600,13 ± 260,36	1444,21 ± 186,85	4207,93 ± 341,63	3924,24 ± 95,78	3212,39 ± 41,29	1234,46 ± 68,15	3866,30 ± 45,26	3633,40 ± 34,04
WE43	Eroded	4413,55 ± 467,13	3883,19 ± 18,16	6489,36 ± 81,93	5500,12 ± 292,11	5052,23 ± 27,9	4023,28 ± 1326,17	6305,09 ± 607,86	6388,44 ± 437,88
	Polished	4557,76 ± 188,30	243,14 ± 4,46	6115,01 ± 264,44	641,94 ± 36,86	5093,77***** ± 2193,2	1061,43 ± 116,56	6420,91 ± 571,12	1202,76 ± 125,53
	Etched	4577,17 ± 186,26	313,97 ± 44,31	5330,31 ± 1067,92	1485,23 ± 364,61	3168,70 ± 28,13	657,21 ± 450,06	4758,18 ± 808,56	1164,68 ± 247,16
E11	Eroded	4994,25 ± 660,48	1065,10 ± 224,90	5409,64 ± 1788,85	2315,59 ± 687,10	4991,89 ± 1561,45	2565,34 ± 340,14	5278,73 ± 336,84	2296,67 ± 1458,13
	Polished	4400,42 ± 317,05	279,58 ± 47,88	3616,09 ± 328,25	1902,95 ± 53,72	2179,65 ± 77,55	465,91 ± 412,07	4553,07 ± 655,87	1247,52 ± 442,99
	Etched	4055,82 ± 164,87	244,65 ± 6,20	3922,77***** ± 910,01	712,07 ± 184,41	2716,70 ± 451,93	326,49 ± 104,77	3894,25***** ± 285,88	1049,59 ± 690,27

Sample	Surface condition	Alloying element	Cumulative release of alloying elements [mg/kg]							
			5 % oxygen				21 % oxygen			
			HBSS	DMEM	HBSS+FBS	DMEM+FBS	HBSS	DMEM	HBSS+FBS	DMEM+FBS
WE43	Eroded	Gd	1.91 ± 1.65	2,69 ± 0,55	4,27 ± 4,90	0	11,24 ± 0,55	7,56 ± 4,75	9,85 ± 0,84	8,32 ± 3,82
		Nd	11,61 ± 6,52	13,83 ± 2,04	18,27 ± 17,30	14,13 ± 0,32	39,43 ± 2,22	25,59 ± 17,19	34,82 ± 3,58	30,10 ± 13,65
		Y	18,85 ± 7,82	22,35 2,94	35,41 ± 33,25	31,00 ± 3,73	60,53 ± 1,14	44,24 ± 32,90	64,85 ± 0,56	45,84 ± 20,04
	Polished	Gd	0,65 ± 0,57	0	1,84 ± 0,51	0	12,77 ± 9,25	1,51 ± 0,79	6,28 ± 3,50	0,33 ± 0,04
		Nd	6,40 ± 2,24	0	10,39 ± 2,419	0	44,82 ± 33,16	3,90 ± 2,88	23,03 ± 12,83	1,43 ± 0,23
		Y	11,85 ± 3,24	0	16,92 ± 3,28	2,52 ± 0,66	64,08 ± 44,27	5,78 ± 4,15	35,56 ± 18,02	2,40 ± 0,28
	Etched	Gd	0	0	2,61 ± 1,72	0	4,36 ± 2,38	0,88 ± 0,49	4,03 ± 4,34	0,17 ± 0,27
		Nd	3,40 ± 0,49	0	12,02 ± 5,69	0	13,81 ± 8,41	1,47 ± 1,78	14,51 ± 15,57	0,79 ± 0,86
		Y	8,12 ± 0,31	0	24,40 ± 12,27	2,60 ± 0,48	24,98 ± 14,52	2,25 ± 2,84	23,74 ± 21,49	1,78 ± 1,51
E11	Eroded	Gd	80,21 ± 78,16	34,23 ± 1,12	175,87 ± 167,34	16,42 ± 5,88	252,61 ± 207,66	27,85 ± 0,37	63,20 ± 17,95	48,32 ± 17,48
		Nd	7,03 ± 6,91	3,34 ± 0,16	16,80 ± 16,21	1,85 ± 0,2	23,42 ± 18,67	2,56 ± 0,05	5,70 ± 1,80	4,61 ± 1,57
	Polished	Gd	35,00 ± 15,20	0	7,17 ± 3,51	0	10,37 ± 0,40	0,52 ± 0,05	32,45 ± 32,67	0,46 ± 0,72
		Nd	3,27 ± 1,51	0	0,73 ± 0,31	0	0,91 ± 0,01	0,04 ± 0,01	2,88 ± 3,08	0
	Etched	Gd	9,48 ± 6,13	0	49,84 ± 50,88	0	55,57 ± 67,33	1,04 ± 0,28	109,32 ± 84,30	29,55 ± 41,75
		Nd	0,66 ± 0,63	0	4,63 ± 4,60	0	5,22 ± 6,46	0,08 ± 0,05	9,78 ± 7,63	2,73 ± 4,03